Pharmacological Research 215 (2025) 107722



Contents lists available at ScienceDirect

Pharmacological Research

journal homepage: www.elsevier.com/locate/yphrs





Targeting USP47 enhances the efficacy of KRAS inhibitor in KRAS^{G12C} mutated non-small cell lung cancer by controlling deubiquitination of c-Myc

Hyungkyung Shin [a,1], SuA Hwang [a,b,1], Jeong Hyun Jeong [c], Sang Chul Shin [d], Yeonji Oh [c], Jinhyeok Kim [c,e], Inah Hwang [a,b], Eunice EunKyeong Kim [c,*], Hyunah Choo [c,e,**], Eun Joo Song [a,b,***]

[a] Graduate School of Pharmaceutical Sciences and College of Pharmacy, Ewha Womans University, Seoul, Republic of Korea
[b] Graduate Program in Innovative Biomaterials Convergence, Ewha Womans University, Seoul, Republic of Korea
[c] Medicinal Materials Research Center, Biomedical Research Institute, Korea Institute of Science and Technology, Seoul 02792, Republic of Korea
[d] Technological Convergence Center, Korea Institute of Science and Technology, Seoul, Republic of Korea
[e] Division of Bio-Medical Science and Technology, KIST School, University of Science and Technology, Seoul 02792, Republic of Korea

ARTICLE INFO

Keywords:
USP47
NSCLC
C-Myc
KRAS
Sotorasib

ABSTRACT

FDA-approved KRAS^{G12C} inhibitors, like Sotorasib, target G12C-mutated KRAS in NSCLC. However, issues with insensitivity and drug resistance have emerged, requiring the development of new combination therapies to overcome these limitations. USP47 has been identified as a regulator of cancer-related signaling pathways such as Wnt, Hippo, and p53. However, its role in the KRAS signaling pathway remains largely unexplored and USP47 inhibitors are less developed than those targeting its homolog, USP7. Here, we identify USP47 as a novel therapeutic target in KRAS^{G12C}-mutated NSCLC and report K-552, a selective USP47 inhibitor, as a potential treatment strategy. We demonstrate that USP47 stabilizes c-Myc by preventing its proteasomal degradation through deubiquitination, thereby promoting NSCLC cell proliferation. Additionally, the compound K-552, a USP47 inhibitor identified through virtual screening, effectively destabilizes c-Myc and inhibits KRAS^{G12C}-mutated NSCLC cell proliferation. Furthermore, USP47 inhibition—either by siRNA knockdown or K-552 treatment—enhances the efficacy of Sotorasib *in vitro* and *in vivo*. Together, our findings establish USP47 as a promising therapeutic target in KRAS^{G12C}-mutated NSCLC and introduce K-552 as a USP47 inhibitor with potential for combination therapy with KRAS^{G12C} inhibitors.

1. Introduction

Despite recent advancements in diagnosis and treatment, lung cancer continues to be the most common cancer in both men and women, with high incidence rates and malignancy when compared to other types of cancer. Non-small cell lung cancer (NSCLC), which accounts for up to 85 % of all lung cancers, comprises two main subtypes: lung squamous cell carcinoma (LUSC) and lung adenocarcinoma (LUAD) [1]. One of the prevalent drivers of lung cancer is a particular KRAS gene mutation [2]. Specifically, the KRAS G12 mutation is a common oncogenic alteration observed in NSCLC, which hyperactivates KRAS-MEK-MAPK signaling pathways leading to increased transcriptional c-Myc activity [3,4]. Consequently, targeting mutant KRAS proteins has emerged as a pivotal therapeutic approach for managing various human cancers with a particular focus on NSCLC. In 2021, the FDA approved Sotorasib, the first small molecule inhibitor targeting the mutant KRAS^{G12C} protein, followed by recently approved Adagrasib [5,6]. Nevertheless, some patients fail to respond adequately to the treatments, while prolonged

* Corresponding author.
** Corresponding author at: Medicinal Materials Research Center, Biomedical Research Institute, Korea Institute of Science and Technology, Seoul 02792, Republic of Korea.
*** Corresponding author at: Graduate School of Pharmaceutical Sciences and College of Pharmacy, Ewha Womans University, Seoul, Republic of Korea.
E-mail addresses: eunice@kist.re.kr (E.E. Kim), hchoo@kist.re.kr (H. Choo), esong@ewha.ac.kr (E.J. Song).
[1] These authors contributed equally.

https://doi.org/10.1016/j.phrs.2025.107722
Received 13 November 2024; Received in revised form 31 March 2025; Accepted 31 March 2025
Available online 1 April 2025
1043-6618/© 2025 The Author(s). Published by Elsevier Ltd. This is an open access article under the CC BY-NC-ND license (http://creativecommons.org/licenses/by-nc-nd/4.0/).

use of $KRAS^{G12Ci}$ has been associated with reduced sensitivity and the development of tolerance to its effects [7–9]. To overcome these issues, concomitant treatments with other drugs alongside Sotorasib are considered to improve Sotorasib efficacy [10–13]. These mainly comprise the inhibitors that target their upstream or downstream proteins, such as SHP2, MEK, or MAPK. Recently, lncRNAs have also been suggested as regulators of the KRAS signaling pathway [14]. An earlier study indicated that the abundance of c-Myc is accompanied by $KRAS^{G12Ci}$ insensitivity in clinical practice [7]. It was also confirmed that c-Myc was the key molecule influencing $KRAS^{G12Ci}$ sensitivity and resistance *in vitro* and *in vivo* models. Therefore, the inhibition of c-Myc is also suggested as another strategy to enhance the sensitivity of $KRAS^{G12Ci}$ [4,15].

c-Myc, a well-known transcription factor, is a central regulator of cell growth and proliferation [16]. It functions as a proto-oncogene and is overexpressed in various cancers, leading to the overexpression of cell-proliferation-related genes and promoting cancer formation. Notably, c-Myc is also overexpressed in NSCLC tissue compared to the adjacent normal epithelium [17,18]. The protein level of c-Myc is regulated through the ubiquitin-proteasome system, where it undergoes ubiquitination by E3 ligases, such as FBXW7, and is subsequently degraded by the 26S proteasome [19]. Consequently, targeting the dysregulated levels of c-Myc has emerged as a promising therapeutic strategy in cancer treatment [20].

Deubiquitinating enzymes (DUB) play critical roles in regulating post-translational modifications and are implicated in various physiological processes, such as protein stabilization, subcellular localization, and protein-protein interactions. Since dysregulation of DUBs has been linked to the development of various cancers [21], developing inhibitors that target DUBs for cancer therapies has attracted attention [22]. USP47, one of the DUBs is involved in a variety of biological processes including cell cycle, neuronal development, viral entry, and inflammation [23]. USP47 is upregulated in various types of cancers [24–28] and regulates many cancer-related signaling pathways, including the Wnt signal, Hippo [29], p53 [30,31], and RAS-MAPK [25,32]. Targeting USP47 with a small molecule inhibitor has emerged as a novel targeted therapeutic approach, as USP47 inhibition led to cell death of hematologic malignancies characterized by mutant EZH2 expression [26]. Other study showed that targeting USP47 could overcome TKI resistance in cancer, suppressing BCR-ABL mutation-induced CML proliferation [25]. Another study revealed a novel USP47/7 dual inhibitor that reduces beta catenin by inactivating USP47 [28,33]. In other words, USP47 inhibitors have been evaluated in CRC, CML, and DLBCL, while their therapeutic potential in combination with $KRAS^{G12Ci}$ in NSCLC remains underexplored. Moreover, USP47 inhibitors are still less developed as an anti-cancer drug compared to other enzymes within the ubiquitin-proteasome system [22,34]. Together, these functional studies on USP47 support its potential as a promising target for anti-cancer therapies, emphasizing the necessity of developing compounds that target USP47.

In this study, we aimed to identify novel substrates of USP47 and evaluate compounds targeting USP47 as a potential cancer therapy. Our results indicated that USP47 facilitates NSCLC cell proliferation by stabilizing the c-Myc protein and blocking proteasomal degradation in vitro. Furthermore, we identified the K-552 compound as an inhibitor of USP47 based on the structure of the USP47 catalytic domain, performing virtual screening, molecular docking study, and *in vitro* experiments [35,36]. K-552 effectively suppresses USP47 activity, leading to c-Myc destabilization and inhibition of NSCLC cell proliferation. Additionally, we co-treated $KRAS^{G12C}$ mutated NSCLC cells with Sotorasib and K-552 to elucidate the enhanced effects on cancer cells *in vitro* and *in vivo*.

In conclusion, our study suggests that USP47 is a promising target for $KRAS^{G12C}$ mutated NSCLC, with K-552 emerging as a compound for USP47 inhibition and a potential candidate for anti-cancer therapy. These findings also indicate that targeting DUBs, including USP47, could be an effective treatment strategy for KRAS driven cancers.

2. Materials and method

2.1. Cell culture

HEK293T cells, A549 cells, Calu-1 cells, H358 cells, and HCC1171 cells were all purchased from Korea Cell Line Bank (KCLB). HEK293T cells were grown as described in our previous study [30]. Other NSCLC cell lines were maintained at the Roswell Park Memorial Institute 1640 (RPMI 1640) supplemented with 10 % fetal bovine serum, 100 units/mL penicillin, and 100 μg/mL streptomycin [37]. Cells were cultured at 37°C in an atmosphere containing 5 % CO_2.

2.2. Plasmids

GFP-tagged c-Myc was purchased from Addgene (catalog number #4704). The coding sequence of c-Myc was cloned into the pCS2 N-terminus HA-tagged vector. pFlag-CMV™-2-USP47, pFlag-CMV™-2-$USP47^{C109S}$ (catalytically inactive mutant), and histidine-tagged ubiquitin plasmids were used as in our previous study [30].

2.3. Transfection

For the DNA plasmid transfection in the NSCLC cell lines, either Effectene (Qiagen) or Lipofectamine 3000 (Invitrogen) was selected and used according to the manufacturer's instructions. For the 293 T cell line transfection, we used the calcium/phosphate/DNA co-precipitation method as described previously [30]. siRNA was transfected using Lipofectamine3000 (Invitrogen, USA). The USP47 siRNA sequence was 5' -TGAAAAGGGATGTGCAAAA-3' (Genolution, Korea). The c-Myc siRNA sequence was 5'-GAGCUAAAACGGAGCUUUU-3' [38].

2.4. Western blot

Samples were lysed with a cell lysis buffer containing 20 mM Tris-Cl (pH 7.5), 150 mM NaCl, 1 mM EDTA, 1 mM EGTA, 1 % Triton X-100, 2.5 mM sodium pyrophosphate, 50 mM NaF, 5 mM β-glycerophosphate, 1 mM Na_3VO_4, and 1X protease inhibitor (cOmplete, EDTA-free; Roche, Basel, Switzerland). The lysate concentrations were evaluated using BCA and calculated using a microplate absorption reader. Lysates were separated with SDS gels and transferred to a nitrocellulose membrane. Membranes were blocked in 5 % skim milk and treated with the primary antibodies diluted in 1 % skim milk at 4°C overnight. After incubation with the second antibody, ECL buffer (Cytivia) was used to develop the membrane.

2.5. Immunoprecipitation

Harvested samples were lysed with the cell lysis buffer. Next, 30 μl of anti-Flag M2 Magnetic beads were incubated with cell lysate for 4 h at 4°C and were washed five times with a wash buffer containing 20 mM Tris-Cl (pH 7.5), 150 mM NaCl, 1 mM EDTA, 1 mM EGTA, 1 % Triton X-100, 2.5 mM sodium pyrophosphate, 50 mM NaF, and 5 mM β-glycerophosphate. After washing, the samples were eluted with Flag peptide and then boiled with 6X sample buffer at 95°C for 5 min. For endogenous immunoprecipitation, rabbit IgG (Cell signaling technology 2729S) or rabbit anti-USP47 antibodies were added into the protein G beads (protein G Sepharose 4 fast flow, GE Healthcare) before being incubated for 1 h. After removing the supernatants, the cell lysate was incubated overnight with antibody-conjugated protein G beads. The samples were eluted with 2X SDS Sample buffer, boiling at 95°C for 5 min. Samples were loaded and separated by SDS-PAGE before being loaded for Western blot.

2.6. Nickel-pull-down assay

Harvested cells were lysed with urea lysis buffer (pH 8.0, 8 M urea,

50 mM Tris, 300 mM NaCl, 50 mM Na_2HPO_4, 1 mM phenylmethylsulfonyl fluoride (PMSF), and 10 mM imidazole), and were sonicated before centrifugation. The samples were incubated with prewashed 70 μg Ni-NTA beads for 4 h in 4°C and then washed five times. Sample elution comprised 2X SDS sample buffer boiling at 95°C before being loaded for Western blot.

2.7. Protein stability test

Indicated plasmids or siRNAs were transfected into A549 cells and treated with cycloheximide at an indicated time. MG132, a proteasomal inhibitor, was treated for 4 h.

2.8. Quantitative real-time PCR (qRT-PCR)

Total cellular RNA was extracted from A549 cells using Trizol. Using ReverTra Ace qPCR RT Master Mix, we synthesized cDNAs and analyzed them with SYBR Green Real-time PCR Master Mix (Toyobo).

The USP47 primers were (F) 5′-ATGGAAGAATCCTGGCACTG-3′ and (R) 5′-CTGGAAGGGATCCAACTTCA-3' [30]. The c-Myc primers were (F) 5'-CCACCTCCAGCTTGTACCTG-3' and (R) 5'-GAGCAGAGAATCCGAGGACG-3'. The β-actin primers were (F) 5'-CACTCTTCCAGCCTTCCTTCC and (R) 5'-CGGACTCGTCATACTCCTGCTT-3' [39]. β-actin was used as a control.

2.9. DUB activity assay using the activity-based probe

A549 cells were seeded in 35 mm culture dishes at 300,000 cells per dish before being incubated at 37°C. DMSO, K-552, and P50429 were diluted in RPMI-1640 media and incubated for 6 h. After the removal of media and washing with cold DPBS, cells were lysed in cell lysis buffer (20 mM Tris-Cl (pH 7.5), 150 mM NaCl, 1 mM EDTA, 1 mM EGTA, 1 % Triton X-100, 2.5 mM sodium pyrophosphate, 50 mM NaF, 5 mM β-glycerophosphate, 1 mM Na_3VO_4, 1X protease inhibitor (cOmplete, EDTA-free; Roche, Basel, Switzerland)). Using a Thermo BCA protein assay kit (Thermo Fischer, Prod# 23235), protein concentrations were calculated using a microplate absorbance reader (Bio-Rad, Hercules, CA, USA). HA-Ubi-PA (UBIQ, UBIQ-078) and 1 mM DTT were added to 60 μg cell lysate before being incubated at 37°C. After 1 h, 6X sample loading buffer (72 mM Tris-HCl (pH6.8), 30 % Glycerol, 2.4 % SDS, 17.28 mM bromophenol blue) was added and the sample was boiled for 5 min at 95°C. Finally, samples were subjected to SDS-PAGE and analyzed by Western blot with the USP47 antibody (Bethyl, A301–904), USP7 antibody (Bethyl, A303–033), with the β-actin antibody (Ab Frontier, LF-PA0207) used as a control.

2.10. Immunofluorescence microscopy

A549 cells were seeded with coverslips and transfected plasmids. After 24 h, cells were harvested, washed with TBS, and fixed with 4 % formaldehyde for 20 min after being washed with Abdil (2 % BSA, 0.1 % Triton X-100 in sterile filtered TBS). Cells were permeabilized for 10 min and then blocked for 10 min. After incubating with the first antibody (Flag M2 antibody, Sigma Aldrich) for 2 h at room temperature, we washed the samples five times and then we incubated with the second antibody (mouse IgG coupled with Alexa-568, Invitrogen) for 1 h at room temperature. Finally, we stained with DAPI for 10 min. The sample was then washed, drained, and mounted. The samples were analyzed using a Zeiss LSM880 Airyscan (Carl Zeiss, Inc., Oberkochen, Germany) at the Ewha Fluorescence Core Imaging Center.

2.11. Colony formation

A549 and Calu-1 were transfected with siRNA targeting USP47 and c-Myc, either alone or together. 500 cells of A549 or 1000 cells of Calu-1 were seeded in 35 mm dishes after 48 h of transfection. And then incubated for nine days. To evaluate the K-552 effect, 500 cells were seeded in a 6-well plate. After two days of incubation, inhibitor compounds were added to each well at the indicated concentrations for 24 h. The media changed every two days. After seven days, samples were harvested. To evaluate the effect of co-treatment of K-552 and Sotorasib, 1000 cells of Calu-1 and 5000 cells of HCC1171 were seeded in 35 mm dishes. After two days of incubation, the inhibitor compounds were treated well at the indicated concentrations for 48 h. The media was changed every two days for 14 days. The harvested samples were fixed with 4 % formaldehyde and cold methanol and then stained with crystal violet.

2.12. Cell proliferation assay (WST-1 assay)

To investigate the effectiveness of K-552, A549 cells were seeded per 96-well, with an inhibitor concentration ranging from 12.5 to 100 μM K-552. To evaluate the synergetic effects of K-552 and Sotorasib, H358, Calu-1 and HCC1171 cells were seeded at 8000(H358), 8000(Calu-1) or 10000(HCC1171) cells per 96-well. After 24 h incubation, inhibitor compounds were incubated at the indicated concentrations for 72 h. EZ-Cytox (DoGEN, EZ-3000) was diluted with media and incubated for 30 min. The absorbance was measured at a wavelength of 450 nm using a microplate absorbance reader (Bio-Rad) (equipped at Ewha Drug Development Research Core Center).

2.13. Apoptosis assay

Calu-1 cell apoptosis was measured using a FITC Annexin V Apoptosis Detection Kit I (BD Pharminge, 556547). Cells were seeded into 60 mm dishes. After 24 h, inhibitor compounds were treated at the indicated concentrations for a further 72 h. Following three gentle washes with cold PBS, cells were collected and centrifuged at 1500 rpm for 2 min at 4°C. Cells were then re-suspended in 1X Annexin V Binding Buffer before the staining solution was. After 30 min incubation, the percentage of apoptotic cells was determined using flow cytometry (FACS Calibur, BD).

2.14. Protein expression and purification

The catalytic domain of *C. elegans* USP47 (Swiss Prot entry: Q22240:1–508 a.a) and human USP7 (Swiss Prot entry: Q93009: 208–560 a.a) were cloned into a pET28a vector, generating an N-terminal His tag. The *c*USP47CD and *h*USP7CD were expressed in *Escherichia coli* BL21(DE3) and purified with an Ni-affinity column. The N-terminal His tag was cleaved by thrombin (Merck) and further purified with a Superdex 200 (GE Healthcare) size exclusion chromatography. The two proteins were purified by checking the purity at each stage on 15 % SDS-PAGE. The purified *c*USP47CD and *h*USP7CDconstructs were concentrated to 20 mg/mL and 25 mg/mL using a VIVASPIN20 (Sartorius) concentrator and stored at −80°C until use, respectively.

2.15. Enzymatic and inhibition assay

USP enzymatic activity and the inhibition assays were measured at room temperature using the cleavage-sensitive fluorogenic substrate Ub-AMC (Boston Biochem, U-550). In the inhibition assays, USP47 (50 nM enzyme) or USP7 (100 nM enzyme) were incubated with varying concentrations (0–100 μM) of K-552 inhibitor in the assay buffer (20 mM HEPES (pH 7.4), 100 mM NaCl, and 5 mM DTT), with 2 % DMSO and UB-AMC (final 35 mM) for 10 min at 25 °C. The AMC fluorescence emission was monitored at 460 nm (excitation at 380 nm) for 30–60 min using a SpectraMax M3 plate reader (Molecular Devices).

2.16. Isothermal titration calorimetry (ITC)

ITC experiments were conducted using the ITC200 instrument

(MicroCal Inc.) and the data were analyzed using the program ORIGIN 7.0. Prior to titration, the protein samples were centrifuged at 18,188 g at 4 °C for 5 min to remove debris. Experiments were carried out by titrating 500 μM K-552 into cells containing 20 μM of prepared $cUSP47_{CD}$ and $hUSP7_{CD}$ protein in an identical buffer with the injectant. The $cUSP47_{CD}$ and $hUSP7_{CD}$ were prepared by dialyzing them in buffer with 20 mM HEPES (pH 7.4), and 150 mM NaCl at 25 °C. The injections were 1.5 μl each, with an injection interval of 150 s. The stoichiometry (n), association constant (K_D), and the change in enthalpy (ΔH), were determined using a nonlinear least-squares curve-fitting algorithm.

2.17. Virtual screening

For virtual screening and molecular docking study, we used the Autodock Vina 4 and Discovery Studio 2020 (Dassault Systèmes). The crystal structures of USP7 (PDB: 5GNE; [40]) and USP47 (PDB: 8ITN and 8ITP; [36]) from the Protein Data Bank (http://rcsb.org/pdb) were prepared using the standard procedure of the Prepare Protein module (CHARMm force field). The binding site of USP7 was defined as an 11 Å radius around the ligand, FT671, while the area overlapping, after superimposing on USP7, was used for USP47. Protonated dockable in-house library molecules and reference ligands were prepared according to rule-based or experimental testing at pH 7.4 and were minimized based on the CHARMm force field. Subsequently, the prepared ligands were docked into the binding site, and molecular docking poses of ligands were obtained using the module CDOCKER Energy.

2.18. Xenograft

All animal procedures were approved by the Institutional Animal Care and Use Committee (IACUC) of Korea Institute of Science and Technology (KIST-IACUC-2022–099–4), and were conducted in accordance with the WMA Statement on Animal Use in Biomedical Research and the EU recommendations (Directive 2010/63/EU), as well as national guidelines for the care and use of laboratory animals. In this study, 4-week-old Balb/c nude male mice (Orient Bio, Korea) were used. The animals were adapted under controlled conditions of constant temperature (22 ± 2 ℃) and humidity (55 ± 5 %). The room lighting was set to automatically turn on and turn off every 12 h (8:00 and 20:00) to keep it constant. To generate an H358 tumor-bearing xenograft model, H358 cells prepared at a concentration of 5×10^6 and mixed with Matrigel (Cat.354230; Corning, NY, USA) were implanted subcutaneously in the right flanks of Balb/c male nude mice. When the tumor size reached 150–200 mm^3, we separated the mice into individual groups: Vehicle, Sotorasib, K552, and Sotorasib + K552 (combination). Sotorasib was dissolved in a solution of 2 % DMSO, 30 % PEG 400, and 0.9 % saline and administered orally at a dose of 3 mg/kg once per day. K552 was dissolved in the same solution as Sotorasib and was administered intraperitoneally at a dose of 10 mg/kg once per day. Tumor volume and body weight were measured daily before drug administration. Tumor volume was calculated by the following formula: Tumor volume (mm3) = [width (mm) x width (mm) x length (mm) / 2. If a tumor exceeds 10 % of the normal body weight, the xenograft experiment was terminated to meet humane endpoint guidelines.

2.19. Histological evaluation

Tumor tissues were harvested and fixed in 4 % paraformaldehyde overnight. After that, the tissues were stored in 30 % sucrose. The tissues were sectioned using a cryostat (CM1850; Leica, Wetzlar, Germany) to a thickness of 20 μm. The tissue was washed three times in distilled water (DW) for 5 min and washed in 1X TBS with 24.7 mM Tris, 0.14 M sodium chloride, 2.7 mM potassium chloride containing 0.025 % Triton X-100 for 10 min. Then, the tissue was rinsed three times in 1X TBS for 10 min. After that, the tissue was incubated in blocking buffer containing 1X TBS and 10 % donkey serum for 1 h at room temperature. The tissue was immersed in an antibody solution in blocking buffer and kept overnight at 4 ℃. The primary antibodies used in this study were as follows: mouse anti-cMyc (diluted 1:200; Santa cruz, Texas, USA), mouse anti-p53 (diluted 1:200; Santa cruz, Texas, USA), rabbit anti-USP47 (diluted 1:100; Abcam, Cambridge, UK), rabbit anti-ki67 (diluted 1:200; Abcam, Cambridge, UK), rabbit anti-cleaved caspase-3 (diluted 1:200; Cell signaling, Massachusetts, USA). Next, the tissue was washed three times in 1X TBS for 10 min and immersed with the secondary antibody in blocking buffer for 2 hr at room temperature. Secondary antibodies used were 488 donkey anti-rabbit, 594 donkey anti-rabbit, and 594 donkey anti-mouse (diluted 1:250; Invitrogen, Carlsbad, CA, USA). Fluorescence signals were detected using a Cytation 5 (Agilent, CA, USA). Morphological changes were assessed using an H&E staining kit (H3502; Vector, CA, USA). The quantification of the mean intensity was performed using the ImageJ software (National Institutes of Health, Bethesda, MD, USA). The mean gray value was measured according to the experiment to be analyzed. To analyze the number of cells, the blind observer excluding the experimenter directly counted the number of cells through the blind test.

2.20. Statistical information

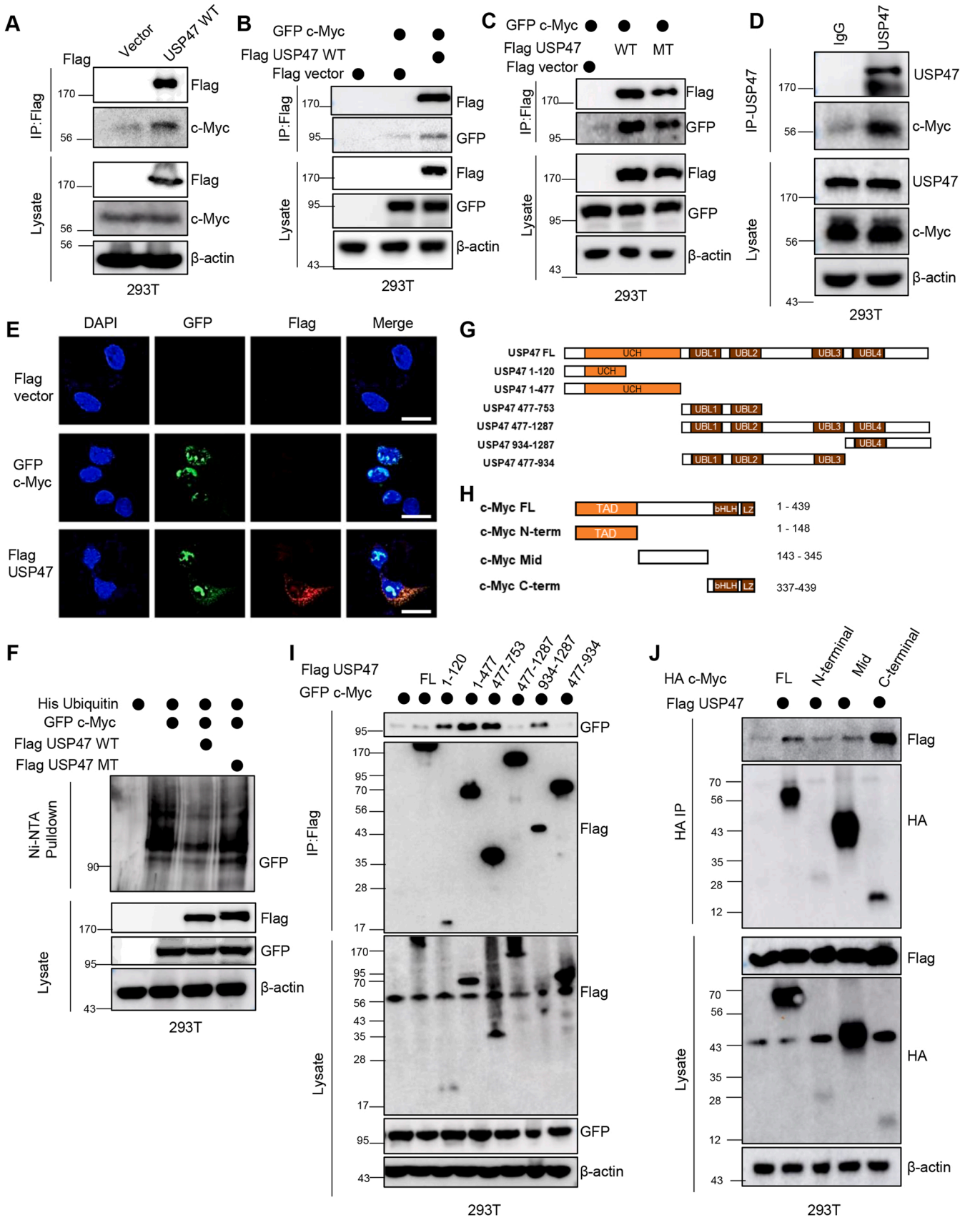
All in vitro and in vivo data were expressed as the mean ± SD or SEM as indicated. For *in vitro* study, the number of replicates was chosen to ensure statistical significance while minimizing experimental variability. For *in vivo* study, sample size was determined based on 'resource equation' [41]. After the experiments, power analysis was conducted using G*POWER to assess the appropriateness of the sample size [42]. Statistical comparisons between two samples were performed using a two-tailed unpaired Student's *t*-test. For analysis involving more than three sample, statistical significance was determined using one-way ANOVA followed by Tukey–Kramer's post-hoc test. A *p*-values below 0.05 were considered statistically significant; (ns, not significant; * *p*-value <0.05; ** *p* value < 0.01; *** *p*-value<0.001; **** *p* -value < 0.001). All statistical analyses were performed using GraphPad Prism (version 9).

3. Results

3.1. USP47 interacts with c-Myc

While high expression levels of USP47 in lung cancer have been reported [27], we try to investigate novel regulatory mechanisms of USP47 to gain a deeper understanding of its role in lung cancer progression. First, we searched UbiBrowser (a database for proteomics on ubiquitin ligase/deubiquitinase substrate prediction) [43] and the synthetic lethal interaction database (Slorth) to find new substrates of USP47, which may provide insights into its regulatory pathways and functions in cancer cells [44]. In these databases, we noted that USP47 might interact with c-Myc and could be associated with KRAS (Figure S1). To examine whether USP47 interacts with c-Myc, we performed immunoprecipitation following the overexpression of Flag-USP47 in HEK293T cells. Our results showed that overexpressed Flag-USP47 binds to both the endogenous and the exogenous c-Myc (Fig. 1A- B). Furthermore, the catalytically inactive mutant Flag-$USP47^{C109S}$ also showed interactions with c-Myc (Fig. 1C). Endogenous USP47 also exhibited binding with c-Myc (Fig. 1D). To determine the subcellular localization of USP47 and c-Myc, we employed confocal microscopy. Interestingly, while GFP-c-Myc was predominantly localized in the nucleolus, we observed co-localization between GFP-c-Myc and Flag-USP47 in both the cytoplasm and the nucleus (Fig. 1E).

To confirm whether c-Myc is deubiquitinated by USP47, we performed a Ni-NTA pull-down assay, which showed a decrease in c-Myc ubiquitination in the presence of USP47 but not $USP47^{C109S}$, despite both binding to c-Myc (Fig. 1F). Then, we conducted a detailed investigation to gain further insights into the interactions between USP47 and



(caption on next page)

Fig. 1. USP47 interacts with c-Myc protein. A HEK293T cells were transfected with Flag-USP47 and the interactions between Flag-USP47 and endogenous c-Myc were detected by immunoblotting after immunoprecipitation with an anti-Flag antibody. B, C HEK293T cells were transfected with GFP-c-Myc and either Flag-USP47 or USP47^{C109S} The interactions between Flag-USP47 and GFP-c-Myc were detected by immunoblotting after immunoprecipitation with an anti-Flag antibody. D The interactions between endogenous USP47 and c-Myc were detected by immunoblotting after immunoprecipitation with an anti-USP47 antibody. E A549 cells were transfected with GFP-c-Myc or Flag-USP47. After incubation with an anti-Flag antibody, samples were immunostained with Alexa Fluor 546 anti-mouse IgG. Co-localization was analyzed by confocal microscopy. Sacle bar = 20 μm. F HEK293T cells were transfected with histidine-tagged ubiquitin, GFP-c-Myc, Flag-USP47, or Flag-USP47^{C109S} for 24 h and treated with 20 μM MG132 for 4 h. Ubiquitinated c-Myc was purified using NI-NTA agarose beads under denaturing conditions and detected with an anti-GFP antibody. G USP47 truncations were used in experiments. H c-Myc truncations used in experiments. I 293 T cells were co-transfected with Flag-USP47 truncations and GFP-c-Myc, followed by immunoprecipitation. J HA-c-Myc truncations and Flag-USP47 were both transfected into 293 T cells for 24 h. Samples were immunoprecipitated using HA agarose beads. All the similar results were observed in three biological experiments.

c-Myc, Specifically, we employed immunoprecipitation to identify the crucial domains of USP47 that facilitate binding with c-Myc, using truncations of Flag-USP47 (Fig. 1G-H) and GFP-c-Myc. Our findings revealed that the UCH domain, which encompasses enzymatic activity, and the UBL1–2 domain, displayed stronger binding to c-Myc compared to the full length USP47. Interestingly, the construction comprising the UBL1–3 and UBL1–4 domains exhibited minimal binding to GFP-c-Myc, despite UBL3 and UBL4 domains revealing binding with c-Myc (Fig. 1I). To identify the interaction domains of c-Myc with USP47, we overexpressed HA-tagged c-Myc truncations with Flag-USP47 and performed immunoprecipitation using HA agarose beads. Our results showed that USP47 binds to c-Myc through the C-terminal domain of c-Myc (Fig. 1J).

3.2. USP47 stabilizes c-Myc by blocking proteasomal degradation

To explore USP47 and c-Myc protein levels in NSCLC cell lines, we performed Western blot analysis on several types of NSCLC cell lines. Our analysis showed that, compared to the wild-type KRAS cell line (H1650), KRAS-mutated NSCLC cell lines—except for H460 (KRAS Q61H)—tended to exhibit higher USP47 protein levels. Furthermore, we observed that KRAS G12-mutated NSCLC cell lines displayed higher levels of both USP47 and c-Myc compared to the wild-type KRAS NSCLC cell line H1650 (Fig. 2A, Figure S2A). Next, we hypothesized that USP47 stabilizes c-Myc protein by preventing its proteasomal degradation in NSCLC cell lines, and we also examined the effect of USP47 on c-Myc protein levels. Among three types of NSCLC cell line (H1650, A549, Calu-1), depletion of USP47 by siRNA levels led to a decrease in c-Myc protein levels, which could be restored by treatment with the proteasome inhibitor MG132 (Fig. 2B, C, Figure S2B). We concluded that depletion of USP47 led to destabilization of c-Myc protein, which appeared to occur regardless of KRAS mutation status. To further investigate the effect of USP47 on c-Myc protein stability, we treated A549 cells with cycloheximide and conducted a time-course analysis. Depletion of USP47 accelerated the degradation of c-Myc protein compared with the control cells (Fig. 2D). Additionally, we examined the impact of USP47 on c-Myc mRNA levels and found no significant alterations induced by deletion of USP47 (Fig. 2E). Conversely, in both A549 and Calu-1 cells, we observed a dose-dependent increase in c-Myc levels upon USP47 overexpression (Fig. 2F, G). But it had no significant alterations on c-Myc mRNA levels induced by overexpressed USP47 (Fig. 2H)

3.3. USP47 inhibition suppresses the proliferation of lung cancer cells by reducing the levels of c-Myc

In our previous study, we found that the depleting USP47 in cancer cells reduced cancer cell viability [30]. This led us to investigate whether the reduction of USP47 affects the phenotype of NSCLC cell proliferation by regulating c-Myc protein levels. To test our hypothesis, we performed a colony formation assay to evaluate changes in cell proliferation among the samples. Consistent with our previous findings, the colony formation assay results showed a decrease in the variety of cancer cell colonies following the knockdown of USP47. However, this decrease was reversed by the overexpression of c-Myc in both A549 and Calu-1 cells (Fig. 3A, B). Additionally, we observed that knockdown of either USP47 or c-Myc reduced cell proliferation. Simultaneous knockdown of both USP47 and c-Myc resulted in a similar reduction in proliferation compared to the single knockdowns. Statistical analysis further revealed that the differences among the knockdown groups were not statistically significant (Fig. 3C-D). These results suggest that USP47 inhibits the proliferation of lung cancer cells by regulating c-Myc protein levels.

We also conducted a bioinformatic analysis to investigate the relationship between USP47 levels and survival rates in lung cancer patients. In the GEO dataset (accession number GSE26939), we observed that the NSCLC patients exhibiting high expressions of USP47 showed significantly lower overall survival rates (Fig. 3E, Figure S3A). Additionally, our analysis of the TCGA-LUAD dataset was consistent with the results of the GEO analysis (Fig. 3F, Figure S3B). Collectively, these findings suggest that targeting USP47 could be a potential therapeutic approach for treating NSCLC, as it reduces survival rates in patients.

3.4. Compound screening shows that K-552 selectively inhibits USP47 in cancer cells

Since the 2000s, the ubiquitin-proteasome system has emerged as a promising target for cancer treatment [34]. The compounds modulating the activities of E3 ligases and DUBs have begun clinical trials [22]. Considering the potential therapeutic mechanism associated with the inhibition of USP47, considerable efforts have been expended on developing USP47 inhibitors in recent years [45,46]. To identify novel USP47 inhibitor compounds, we conducted a compound screening using our compound library using the crystal structures of USP47 (PDB: 8ITN and 8ITF [36]) as well as the USP7 complexed with FT671 (PDB: 5NGE; [40]. Compound selection was based on in silico virtual screening using Autodock Vina and the CDOCKER module in the Discovery Studio software package (Accelrys, Inc.). Initially, we docked over 1000 in-house compounds to the catalytic binding site of USP47 using Autodock Vina, which showed that K-389 had the best binding affinity. Subsequently, we conducted a docking analysis of 40 in-house compounds structurally similar to K-389 utilizing the CDOCKER module. From these analyses, we selected the five compounds with the most favorable CDOCKER Energy scores for inhibiting USP47 activity (K-389, K-565, K-550, K-552, and K-407). We then evaluated their inhibitory potential by employing the activity-based probe HA-Ub-PA and visualized the activity against USP47 and USP7 through immunoblotting. Among the five compounds evaluated, K-552, 9-(3-(4-(2-methoxyphenyl)piperazine-1-yl)propyl)-9H-carbazole, displayed a decrease in the probe-labeled band intensity, which was shown at upper band (HA-Ubi-USP47), for USP47 (Fig. 4A, Figure S4A). Interestingly, the docking pose of K-552 in the catalytic site of USP47 differed significantly from that of USP7, possibly due to the distinct 3D alignments of the two proteins (Figure S4B-C). Subsequently, we evaluated K-552 using Ub-AMC and Ub-PA assays with the catalytic domain of recombinant proteins. The results showed that K-552 inhibited both *c*USP47$_{CD}$ and *h*USP7$_{CD}$, albeit to a greater degree for *c*USP47$_{CD}$ than *h*USP7$_{CD}$ (Fig. 4B, Figure S4D-E). Further evaluation using the HA-Ub-PA probe demonstrated a dose-dependent inhibition of USP47 with K-552 treatment. In Fig. 4C, the results demonstrated a decrease in the upper band, corresponding to the probe-bound USP47 band, with an increasing

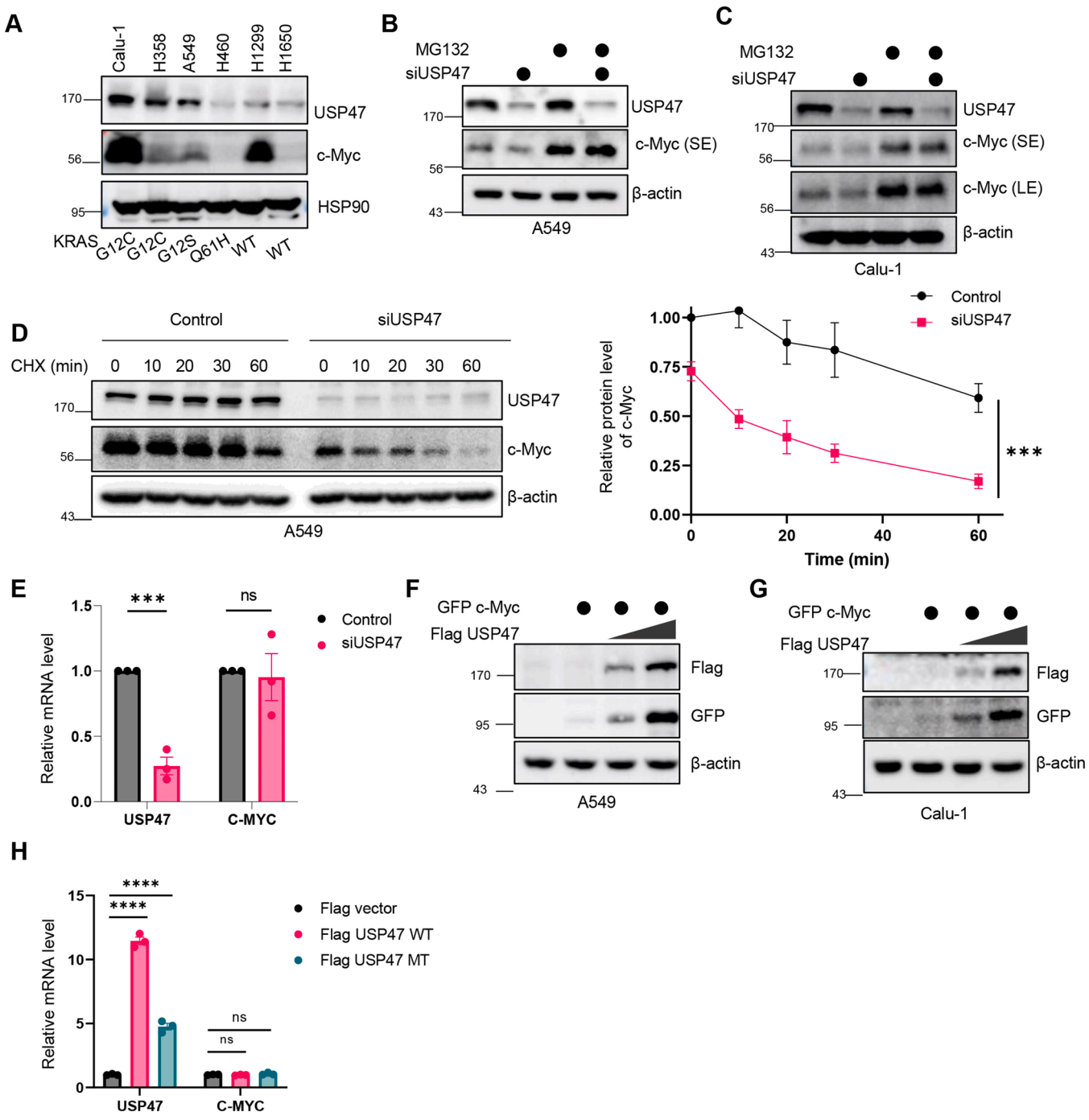


Fig. 2. USP47 deubiquitinates and stabilizes the c-Myc protein level by protecting proteasomal degradation. A Cell lysate was extracted from NSCLC cell lines with different KRAS statuses, and USP47 was analyzed by Western blotting. HSP90 was used as a control. B, C After the transfection of USP47 siRNA in A549 and Calu-1 cells, the cells were treated with 20 μM MG132 for 4 h and immunoblotted with the indicated antibodies. D USP47 siRNA was transfected for 48 h, followed by incubation with 20 μg/mL cycloheximide for the indicated times. β-actin was used as a control for Western blotting. E USP47 siRNA was incubated for 48 h, and qRT-PCR was conducted to investigate the mRNA levels of c-Myc. F, G A549 and Calu-1 cells were transfected with GFP-c-Myc either alone or in combination with different concentrations of Flag-USP47. Western blot analysis was performed to detect GFP-c-Myc protein levels. H Flag-USP47 or USP47^{C109S} was transfected to extract mRNA using Trizol, and the mRNA levels of USP47 and c-Myc were analyzed by qRT-PCR. All western blots results were obtained independently three times biological experiment. qRT-PCR was independently conducted three times.

concentration of K-552. In contrast, no significant changes were observed for HA-Ub-USP7, indicating that USP7 activity remains unaffected by K-552 treatment compared to the DMSO treated sample as a control. Next, we measured the K-552 (500 μM) binding affinity of cUSP47$_{CD}$ (20 μM) and hUSP7$_{CD}$ (20 μM) using ITC, respectively. The ITC results showed the binding affinities for K-552 on the cUSP47$_{CD}$ are about 4-fold lower than that of hUSP7$_{CD}$, with K_D values of 12.3 ± 1.6 μM and 47.3 ± 6.2 μM, respectively (Fig. 4D). Collectively, these results suggest that the K-552 compound shows more specific interactions with cUSP47$_{CD}$ than hUSP7$_{CD}$.

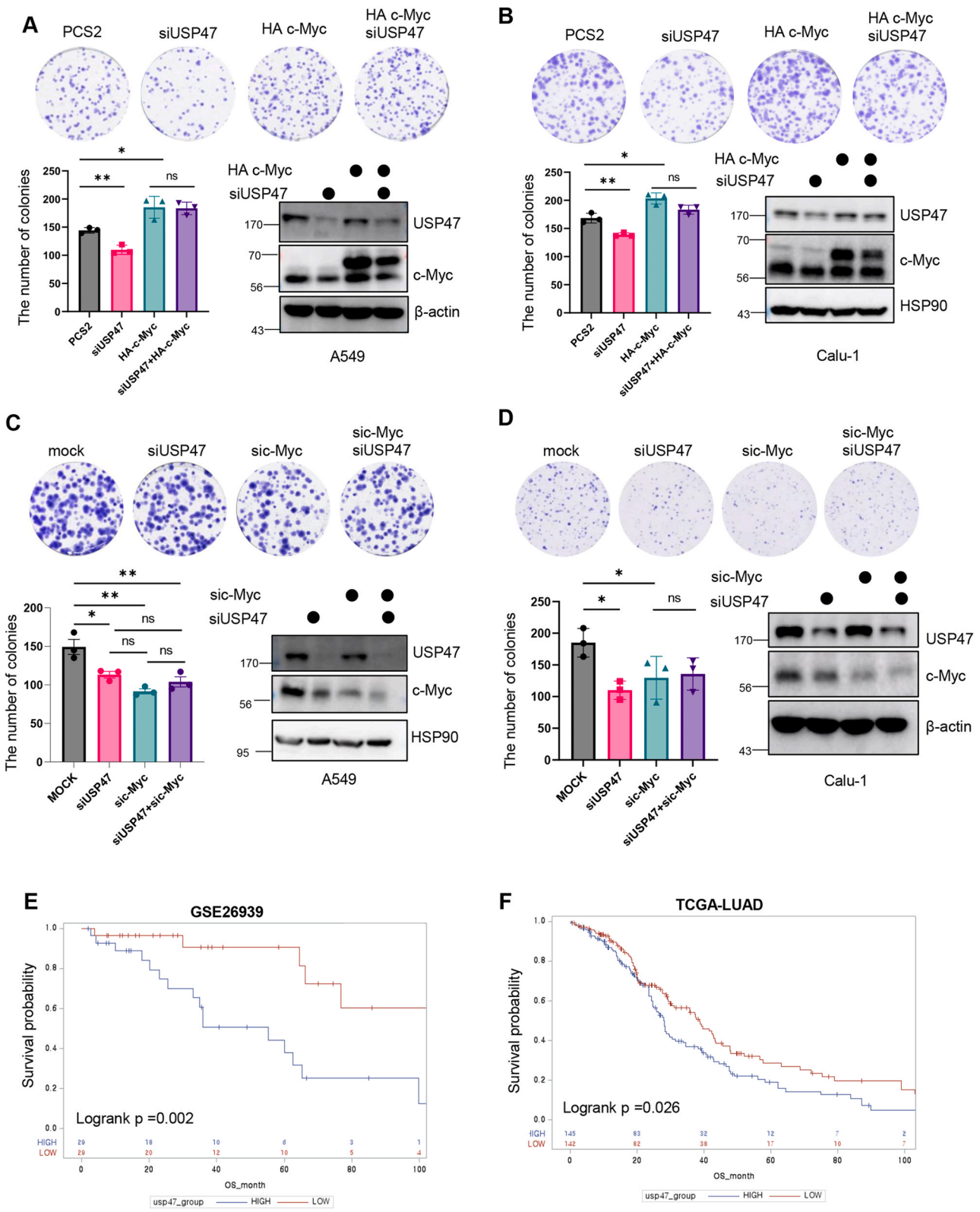
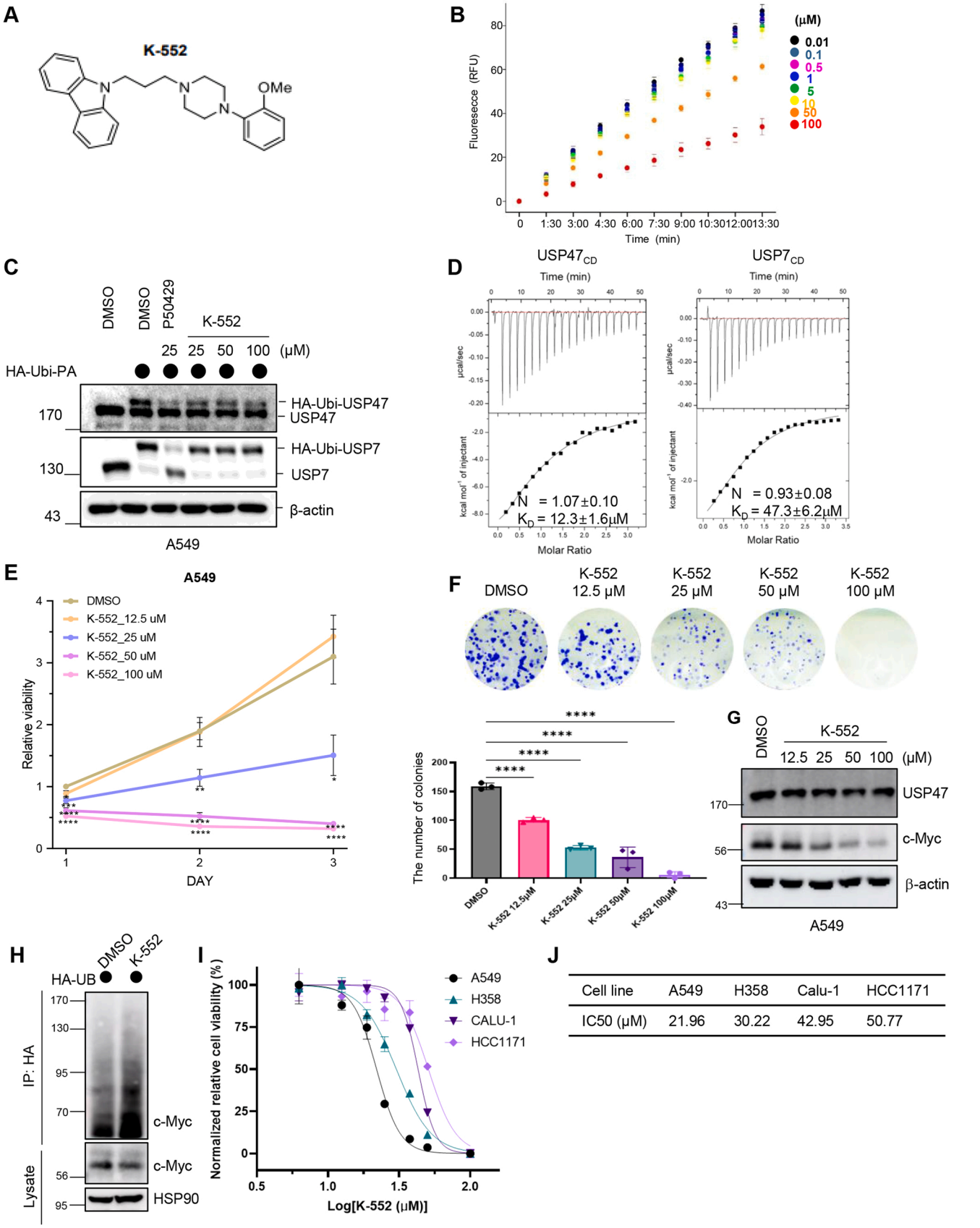


Fig. 3. USP47 influences the proliferation of NSCLC cells and the overall survival of patients. A, B A549 cells and Calu-1 cells were transfected with siUSP47 or HA-c-Myc for 48 h. Subsequently, A549 cells or Calu-1 cells were seeded into a 6-well plate and incubated for 10 days. Colony samples were fixed with 4 % paraformaldehyde in PBS and methanol, before being stained with crystal violet. Additionally, samples were immunoblotted to confirm the levels of the indicated proteins. C, D A549 cells and Calu-1 cells were transfected with siUSP47 or sic-Myc for 48 h, before being seeded into a 6-well plate. After 10 days, the samples were fixed with 4 % paraformaldehyde in PBS and methanol before being stained with crystal violet. Samples were also immunoblotted to confirm the levels of the indicated proteins. Each assay was performed in triplicate in at least three independent experiments for each cell line. E The GSE26939 dataset was used to analyze the survival curve using the SAS Enterprise Guide 8.3 program. F Survival curve analysis was performed using the TCGA-LUAD data downloaded from UCSC Xena, with the SAS Enterprise Guide 8.3 program. The KM plot with survival curve was analyzed by the SAS Enterprise Guide 8.3 program. Log-rank $p < 0.05$ is statistically significant. All western blots results were obtained independently three times biological experiment.



(caption on next page)

Fig. 4. K-552 inhibits USP47 in a dose-dependent manner. A Chemical structure of K-552. B K-552 inhibited the Ub-AMC hydrolysis activity of the cUSP47 catalytic domain: K-552 exhibited detectable inhibition in a dose-dependent manner (0.01 μM to 100 μM). C A549 cells were treated with the indicated concentrations of K-552 for 6 h. Cell lysates were incubated with an activity-based probe, HA-Ubi-HA, and then immunoblotted with the indicated antibodies. β-actin was used as a loading control. D ITC binding curve of K-552 to the catalytic domain. The lower panel shows the integrated heat data against the molar ratio of K-522 to cUSP47CD and *h*USP7CD. The closed squares are fitted to a one-site model, and the solid lines represent the best-fit results. E A549 cells were treated with K-552 at the indicated concentrations. Cell viability was measured using WST-1 assay every 24 h for three days. Each assay was performed in triplicate in at least three independent experiments. F A549 cells were seeded into a 6-well plate and incubated with K-552 at the indicated concentration. After 24 h, the fresh media was replaced every two days for a week. G To elucidate the mechanism of K-552, A549 cells were treated with K-552 for 24 h, and then the samples were analyzed by Western blot using the indicated antibodies. β-actin was used as a loading control. H A549 cells were transfected with HA-tagged ubiquitin for 24 h and treated with 25 μM K-552 for 24 h and 20 μM MG132 for 4 h. Ubiquitinated c-Myc was purified using HA agarose beads under denaturing conditions and detected with an anti-c-Myc antibody. I, J After KRAS G12-mutated NSCLC cells (A549, H358, Calu-1, HCC1171) were treated with K −552 for 72 h, Cell viability was measured using WST-1 assay. And then IC50 was calculated using Prism 9.0.

3.5. K-552 inhibits lung cancer cell proliferation in a dose-dependent manner

We next investigated the effect of K-552 on the viability of A549 lung cancer cells. Using the WST-1 cell proliferation assay, we evaluated cell viability 1, 2, and 3 days after treatment with varying concentrations of K-552. The results revealed that K-552 treatment reduced cell growth compared with the control group. We observed that 12.5 μM K-552 did not significantly affect cell viability, whereas 25 μM K-552 substantially inhibited cell growth after 48 h of treatment. Moreover, treatment with 50 μM and 100 μM of K-552 resulted in a more pronounced effect on cell viability (Fig. 4E). To further confirm the inhibitory effect of K-552 on cell proliferation, we conducted a colony formation assay and WST-1 cell viability test. The results of the colony formation assay showed that treatment with K-552 led to a significant decrease in the number of colonies compared with the control group (Fig. 4F). We also observed a more pronounced reduction in colony formation when higher concentrations of K-552 were treated, suggesting that K-552 inhibits lung cancer cell growth in a dose-dependent manner. Based on our findings, we hypothesized that K-552, through its inhibition of USP47, would also induce c-Myc destabilization by inhibiting deubiquitination of c-Myc protein. As shown in Fig. 4G, treatment of K-552 dose-dependently reduced protein levels of c-Myc. Also, treatment of K-552 increased ubiquitinated c-Myc protein level (Fig. 4H, Figure S5A). Furthermore, each cell viability was decreased in four types of NSCLC cell lines, characterized by $KRAS^{G12S}$ (A549) and $KRAS^{G12C}$ (H358, Calu-1, and HCC1171). We then calculated the IC_{50} values of these results. Interestingly, it was observed that H358, Calu-1, and HCC1171 showed higher IC_{50} values compared with the A549 cell line. According to the K-552 IC_{50} value, we found that Calu-1 and HCC1171 cells display lower sensitivity compared to A549 and H358 (Fig. 4I, J). In conclusion, our findings suggest that K-552 suppresses the proliferation of lung cancer cells by inhibiting USP47 activity, which subsequently prevents c-Myc deubiquitination.

3.6. USP47 positively associates with the KRAS signaling pathway

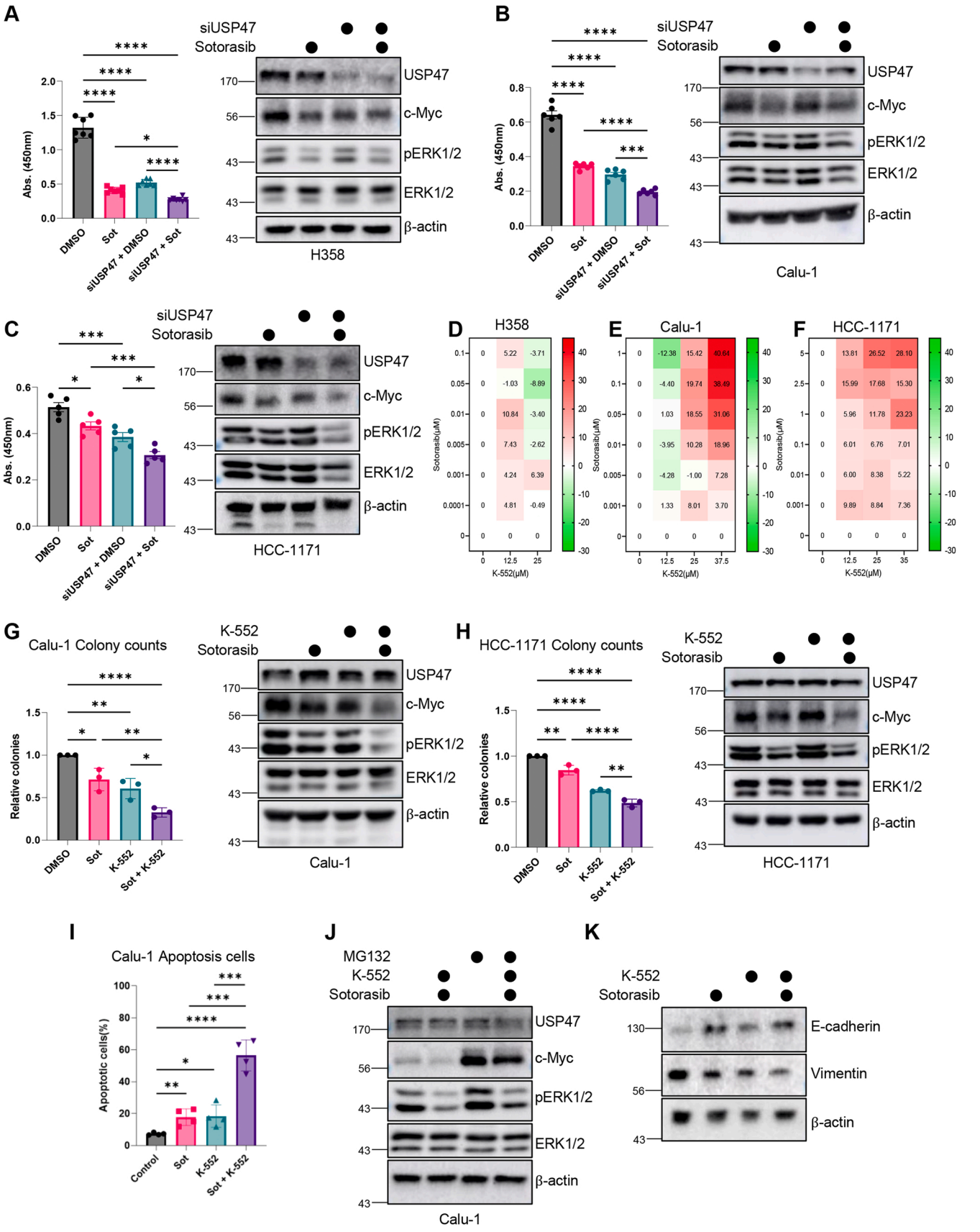
The oncoprotein KRAS is frequently overexpressed and mutated in lung cancer cases, with KRAS mutations accounting for approximately 25 % of NSCLC cases [47]. Previous reports indicate that USP47 is upregulated in lung cancer tissue [48]. Notably, both USP47 and c-Myc exhibit crosstalk with KRAS at various levels. In *Drosophila*, it has been demonstrated that USP47 plays a role in stabilizing MAPK, which serves as a downstream signal of KRAS [32]. In addition, USP47 is regulated by BCR-ABL through the RAS/ERK signaling pathway, with Pan-KRAS inhibitor and ERK inhibitor reducing USP47 protein levels in the CML cell line [25]. c-Myc stability is also regulated by the KRAS signaling pathway [3,4]. Additionally, we noted the possibility of a synthetic lethal interaction between KRAS and USP47 after consulting the proteomics database (Figure S1A), which prompted us to investigate whether there was a correlation between KRAS and USP47 in lung cancer. Analyzing datasets from TCGA-LUAD and the GEO database indicated that the group with high KRAS mRNA expression exhibited higher levels of USP47 mRNA compared with the low KRAS group. Furthermore, there was a significant positive correlation between USP47 and KRAS mRNA expression level ($p < 0.0001$) (Figure S6A-D). Consistent with these results, gene set enrichment analysis (GSEA) showed that USP47 exhibits a positive correlation with the KRAS signaling pathway upregulated in NSCLC (Figure S6E). As mentioned above, the USP47 protein is enriched in oncogenic KRAS-mutated lung cancer cell lines (Fig. 2A, Figure S2A). We, therefore, propose that targeting both oncogenic KRAS G12C mutation and USP47 may represent an effective therapeutic strategy for the treatment of NSCLC patients.

3.7. USP47 inhibition enhances the anti-proliferative effect of Sotorasib in KRAS-mutated lung cancer cells

Based on the correlation we observed between KRAS, USP47 (Figure S6), and c-Myc, we assumed that USP47 could be a target molecule for oncogenic KRAS-mutated NSCLCs. We then focused on targeting USP47 with $KRAS^{G12Ci}$ Sotorasib, the first drug to target KRAS-mutated NSCLC. First, based on the earlier studies, we selected three types of G12C-mutated NSCLC cell lines, namely H358, Calu-1, and HCC1171. Research has shown that H358 is sensitive to Sotorasib, with an IC_{50} of less than 0.1 μM. Although IC_{50} values of Calu-1 and HCC1171 were not obtainable from previous studies experiments [49,50], Calu-1 and HCC1171 exhibit intermediate sensitivity to Sotorasib, showing dose-dependent response to the drug but not achieving sufficient efficacy to the drug. Thus, H358 was chosen as a sensitive cell line to Sotorasib, and Calu-1 and HCC1171 were selected as moderate cell lines to Sotorasib. Correspondingly, we observed that H358 is sensitively responsive to Sotorasib, while Calu-1 and HCC1171 are less sensitive than H358 (Figure S7A-C).

Next, we investigated the incremental effect of $KRAS^{G12Ci}$ Sotorasib with USP47 knockdown to examine whether USP47 is a potential molecule for enhancing the sensitivity of $KRAS^{G12Ci}$ when USP47 decreased with and thereby finding additional effects on cell viability. The cell viability results showed that treatment with both USP47 siRNA and Sotorasib leads to more enhanced suppression compared with either USP47 knockdown or Sotorasib treatment alone in KRAS G12C mutated NSCLC cell lines (Fig. 5A-C). Also, we investigated the mechanism underlying these effects by examining the protein expression levels in cells treated with USP47 siRNA and Sotorasib. Depletion of USP47 using siRNA resulted in a decrease in c-Myc levels. Furthermore, when cells depleted of USP47 were treated with Sotorasib, c-Myc expression levels were reduced when compared to individual treatments (Fig. 5A-C).

Then, we hypothesized that inhibiting USP47 in combination with Sotorasib could serve as a promising strategy to enhance sensitivity in KRAS G12C mutated NSCLC therapy. To test our hypothesis, we examined the effects of inhibiting both USP47 and KRAS G12C on cell viability, particularly in cell lines with KRAS mutations, using the Sotorasib and K-552. The concentration ranges were selected based on the different drug responsiveness of each cell line. As shown in Fig. 4I, J, higher concentrations of K-552 were applied to Calu-1 and HCC1171 (up to 37.5 μM or 35 μM, respectively) compared to H358 (up to 25 μM). The treatment range of Sotorasib was determined based on previous



(caption on next page)

Fig. 5. Co-treatment of Sotorasib and K-552 in KRAS G12C mutated NSCLC cell line. A-C KRAS G12C-mutated NSCLC cells (H358, Calu-1, HCC1171) were treated with 0.1 μM Sotorasib and siUSP47 for 72 h. Cell viability is presented with the value of absorbance (mean ± SD). Immunoblot analysis of proteins from H358, Calu-1 and HCC1171 cells treated with Sotorasib and USP47 siRNA. D–F Bliss Synergy Score (BSS) was calculated using SynergyFinder 3.0 with the results of Sotorasib and K-552 as indicated concentration (Fig. S5 A-C G-H) G, H Colony formation assay was conducted on KRAS G12C-mutated NSCLC cells (Calu-1, HCC1171) grown under Sotorasib (0.1 μM) and K-552 (25 μM). The number of colonies is shown relative to untreated controls (mean ± SD). Each assay was performed in triplicate in at least three independent experiments for each cell line. Statistical significance for the relative colony number was assessed using an ANOVA, with $*p < 0.05$, $**p < 0.01$, $**p < 0.001$, and $****p < 0.0001$ denoting the significance levels. Immunoblot analysis of several proteins was performed on Calu-1 and HCC1171 cells and inhibitor compounds were treated as the same as the colony formation. I Annexin V-FITC/PI staining was conducted on KRAS G12C mutated NSCLC cells treated on Sotorasib and K-552 of same concentrations as the colony formation for 72 h. The percentage of apoptotic cells was determined using flow cytometry. J 20 μM MG132 is treated with concomitant therapy both 0.1 μM Sotorasib and 25 μM K-552 for 8 h in Calu-1 cell which is mutated in KRAS G12C and then immunoblotted with the indicated antibodies. K To check for changes in EMT marker protein following treatment with 0.1 μM Sotorasib and 25 μM K-552 alone or together for 8 h, immunoblot analysis was performed with the indicated antibodies. All western blots results were obtained independently three times biological experiment.

studies [49,50]. For H358, the Sotorasib concentration range was set to 0–0.1 μM, which is below its IC_{50}. Sotorasib was treated on Calu-1 and HCC-1171 at the indicated ranges [49,50]. Our results showed a significant reduction in cell viability in KRAS G12C-mutated NSCLC cell lines following treatment with each compound. Furthermore, we observed an additional reduction in cell viability with combination treatment compared to treatment with either Sotorasib or K-552 (Figure S7A-C) and determined its synergistic effect, calculated by the Bliss Synergy Score (BSS) [51]. Since Sotorasib exhibits a more pronounced effect in the H358 cell line, K-552 cotreatment has a comparatively weaker synergistic effect than it does in the other Sotorasib-moderate cell lines, Calu-1 and HCC1171 (Fig. 5D-F). To explore effects of the combination therapy, we conducted a colony formation assay on the two types of NSCLC treated with either Sotorasib or K-552 individually or in combination. We observed a reduction in colony formation when either Sotorasib or K-552 was used. Notably, the combination treatment of Sotorasib and K-552 resulted in a significant decrease in colony formation. These results provide evidence for the additional effect achieved by combining Sotorasib and K-552 in inhibiting colony formation. (Figure S7D, E, Fig. 5G-H).

To investigate whether the decrease in cell viability and colony formation observed with the co-treatment of Sotorasib and K-552 is attributable to apoptosis, we conducted an analysis of cell apoptosis using flow cytometry with Annexin V-FITC/PI staining. The results showed a significant increase in early and late apoptosis when the cells were treated with Sotorasib and K-552 either individually or in combination. Moreover, the combination treatment of Sotorasib and K-552 resulted in a more pronounced increase in apoptosis compared with the individual treatments (Fig. 5I, Figure S7G).

We also investigated the molecular mechanism underlying the combined treatment by examining the levels of pERK and c-Myc using immunoblotting. The combination of Sotorasib and K-552 resulted in a further reduction in c-Myc levels (Fig. 5G, H). Moreover, the effect was more pronounced compared with the individual administration of Sotorasib or K-552, as the results were seen for Sotorasib with siUSP47 (Fig. 5A-F). These findings provide additional evidence for the enhanced therapeutic impact achieved through combining Sotorasib and K-552 treatments, highlighting the synergistic modulation of c-Myc expression levels (Fig. 5C-D). To explore whether the decrease in the c-Myc level is associated with degradation, we examined the c-Myc level following the treatment of MG132 or chloroquine, inhibitors of proteasome or autophagy, respectively. c-Myc level was recovered by treatment with MG132 but not with chloroquine (Fig. 5J, Figure S7H). These results indicate that c-Myc protein levels are mediated by ubiquitin proteasomal degradation rather than the autophagic pathway. Furthermore, we confirmed that Sotorasib and K-552 reduce epithelial-to-mesenchymal transition (EMT) protein markers, which are responsible for cancer cell migration and enhanced growth (Fig. 5K). In summary, co-treatment of K-552 with Sotorasib both increases and sensitizes the medication's effectiveness in NSCLC cells.

3.8. The combination of Sotorasib and K552 is effective in the KRAS-mutant NSCLC in vivo model

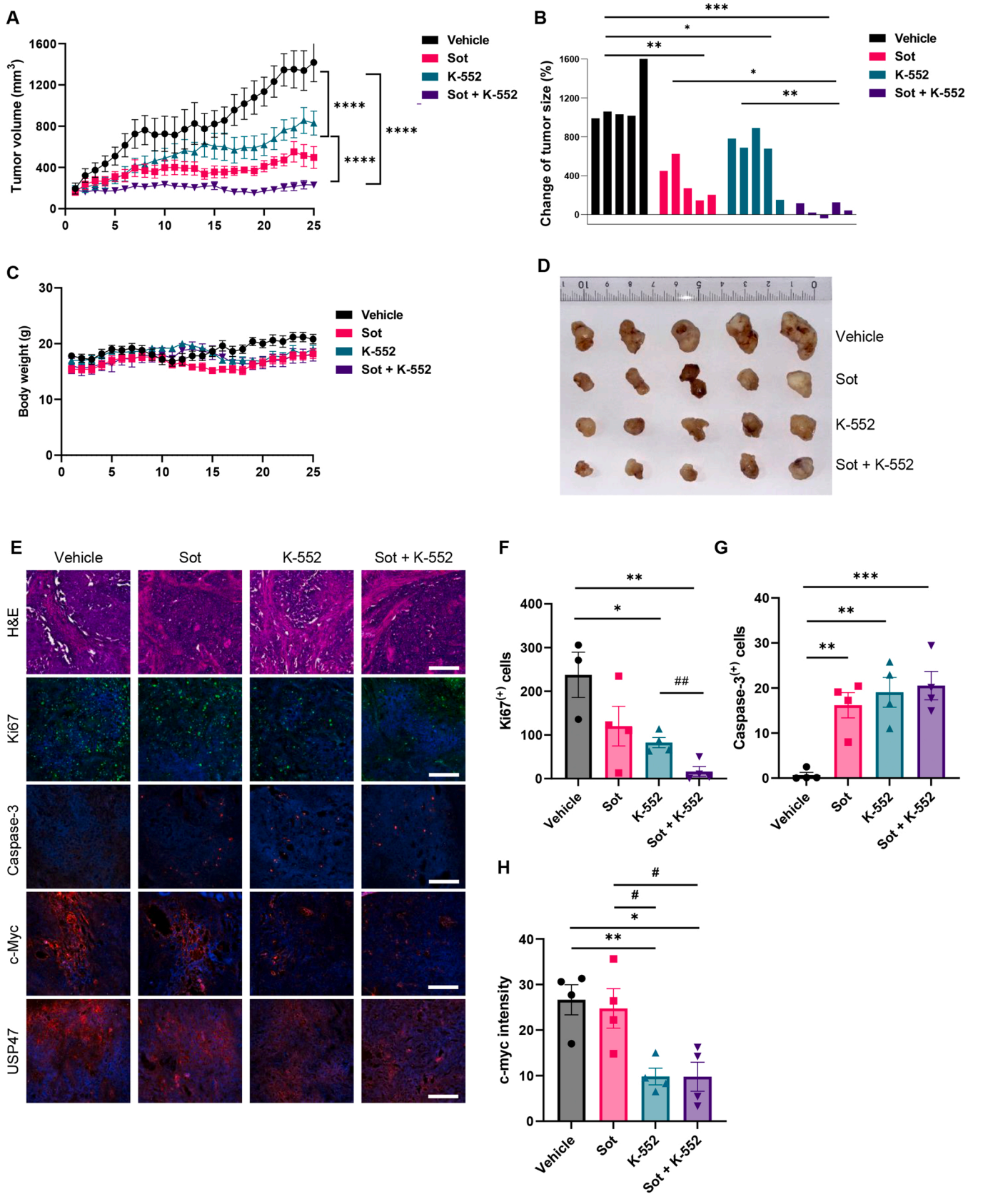
To evaluate the effects of Sotorasib, K-552, and their combination on tumor growth delay *in vivo*, we generated a xenograft model using H358 cells chosen for their sensitivity to Sotorasib (Fig. 5). Following the inoculation of H358 cells into the mice, we randomly divided them into four groups and administered the drugs when the tumor volume reached 150–200 mm^3. Subsequently, we monitored tumor growth and body weight for a period of 25 days. Results indicate that both Sotorasib and K552, individually and in combination, delayed tumor growth, with a decreased growth rate observed in all treatment groups compared to the vehicle group. Moreover, the combination treatment exhibited statistically significant additional effects on tumor growth inhibition compared to the treatment of each drug (Fig. 6A-B). During the experiment, when measuring the body weight of the mice, the vehicle group tended to gain more weight compared to each drug treatment group. This is thought to be due to the increased tumor tissue weight in the vehicle group (Fig. 6C). We obtained all the tumor tissues on day 25 after the drug administration and observed that tumor size decreased in all treatment groups compared to the vehicle group (Fig. 6D). To sum up, we discovered that both K-552 (USP47 inhibitor) and Sotorasib have collaborative effects of tumor suppression *in vivo*.

Next, we evaluated the effects of Sotorasib and K552 on cell proliferation and apoptosis in the tumor tissues using immunofluorescence staining with Ki67 for proliferation and cleaved caspase-3 for apoptosis and tumor suppression. As in Fig. 6E, we determined that the combination treatment of Sotorasib and K552 decreased the number of ki67-positive cells, and several caspase-3-positive cells compared to other groups and the combination (Fig. 6 F-G).

To mechanistically validate the on-target effect of combined Sotorasib and USP47 inhibition *in vivo*, we assessed the levels of USP47 and c-Myc using immunofluorescence staining. Consistent with the cell line results, USP47 inhibition led to a decrease in c-Myc levels. In the Sotorasib-treated tumor tissue, c-Myc levels were almost similar to those in the vehicle group. However, co-treatment with K552 and Sotorasib resulted in a significant decrease in c-Myc levels (Fig. 6E-H). This implies that while Sotorasib treatment reduces c-Myc levels *in vitro*, Sotorasib treatment *in vivo* may allow c-Myc levels to rebound to those of the vehicle group. The combination with K-552 helps maintain reduced c-Myc levels over time, supporting its potential to enhance the sustained effects of Sotorasib. All these results showed that the combination treatment of Sotorasib and K552 had more pronounced effects compared to the individual treatment with Sotorasib or K552 and that the combination treatment of Sotorasib and K552 delayed tumor growth, inhibited cell proliferation, and increased cell apoptosis by inhibiting USP47 and destabilizing c-Myc. Taken together, these findings provide valuable insights into the potential therapeutic benefits of using both Sotorasib and USP47 inhibitors in the treatment of NSCLC.

4. Discussion

USP47 has emerged as a promising therapeutic target for the



(caption on next page)

Fig. 6. Co-treatment of Sotorasbib and K-552 shows synergetic effects on NSCLC treatment in a xenograft mouse model. A-C H358 cells were inoculated into Balb/c nude mouses. After 7days of inoculation, we divided into 4 groups (Vehicle, Sotorasib, K-552, combination treatment) and measured tumor volumes, and body weight for 25 days. The graphs indicate tumor volume, the rate of tumor growth, and body weight in the H358 tumor-bearing xenograft model. D After the end of treatment, the mice were sacrificed and then tumors were harvested. The representative image shows tumor formation in vehicle group and each treatment group. E The harvested tumors were immunostainned and then imaged using confocal microscope. The representative image shows morphological changes, Ki67, Caspase-3 USP47 and c-Myc immunoreactivity. Scale bar = 200 μm. F The bar graph indicates quantification of the number of Ki67 positive cells (mean ± SEM; n = 4 from each group). G The bar graph indicates quantification of the number of Caspase-3 positive cells (means ± SEM; n = 4 from each group). *$p < 0.05$ vs. the vehicle group. H Bar graph indicates quantification of the immunofluorescence intensity of c-myc (mean ± SEM; n = 4 from each group). *$p < 0.05$, **$p < 0.01$, ***$p < 0.001$, ****$p < 0.0001$ vs. the vehicle groups, $p < 0.05$ vs. combination of the Sotorasib and K552 group, $p < 0.0001$ vs. each of the Sotorasib and K552 group.

treatment of cancer, as it is upregulated in various cancers such as colon cancer, acute myeloid leukemia, and lymphoma. Specifically, USP47 is upregulated in NSCLC patients [27], while inhibitors targeting Pan-KRAS or pERK reduce USP47 protein levels in CML [26]. In the Drosophila model, USP47 regulates MAPK stability, although the underlying mechanism remains unknown [32]. Additionally, another study found that USP47 positively correlates with and activates NF-κB [52], which is linked to the KRAS/PI3K/AKT signaling pathway and is part of the MAPK signaling pathway [53]. These findings suggest that targeting USP47 could be an effective strategy against NSCLC and may reveal additional functions of USP47 within the KRAS signaling pathway. In this study, we focused on elucidating the role of USP47 in KRAS G12C-mutated NSCLC. First, we investigated the potential functional mechanism of USP47 in the NSCLC cell line and found that as a substrate of USP47, c-Myc is stabilized, leading to USP47-mediated cell proliferation in NSCLC cells (Figs. 1 and 2). Furthermore, we identified the K-552 compound as a USP47 inhibitor based on USP47 protein structure we discovered before, which induced cell death in KRAS G12C-mutated NSCLC cells (Fig. 4). Finally, we showed that Sotorasib, a KRAS G12C inhibitor, with USP47 inhibitor K-552 results in an additive effect on growth inhibition of KRAS G12C-mutated NSCLC both *in vitro* and *in vivo* (Figs. 5 and 6).

Early studies have shown that several DUBs, including USP28 [54], USP7 [55], USP37 [56], USP36 [57], USP43 [58], OTUD6A [59] stabilize c-Myc through deubiquitination. Most of these DUBs (such as USP28, USP36, USP38, and OTUD6A) specifically interact with c-Myc in the transactivation domain (TAD), where the well-known c-Myc targeting E3 ligases FBXW7 primarily binds [19,60]. In contrast, USP37 regulates and interacts with c-Myc independently of the TAD domain [56]. USP43 binds to both the N-terminal and C-terminal domains of c-Myc [58]. In this study, we observed that USP47 primarily binds to the C-terminal domain of c-Myc, unlike other DUBs known for targeting c-Myc. USP47 may deubiquitinate c-Myc that has been ubiquitinated not only by FBXW7 but also by other E3 ligases, suggesting that USP47 could play a crucial role in stabilizing c-Myc.

We also discovered that c-Myc interacts with USP47's catalytic domain, as well as the UBL1 and UBL2 domains of USP47 (Fig. 1I). Our previous study discovered that RPS2 directly interacts with $USP47^{477–934}$, which contains UBL1–3 domain [61]. However, the interaction between USP47 and c-Myc disappeared in $USP47^{477–934}$ and $USP47^{477–1287}$ which are deleted the catalytic domain or UBL4 domain, suggesting distinct roles for USP47 domains. This implies that USP47 domains have different roles from their substrates. It is plausible that USP47 UBLs may function different substrate binding affinity, affect structural changes or enzymatic activity. USP7, which is reported to homology with USP47 [62], organizes its UBL domain 2–1–2 differently and regulates its activity through the conformation change [62]. Also, the N-terminal UBL domain of USP4 is reported to affect the enzymatic activity of USP4 *in vitro* [63]. Based on these, it is tempting to suggest that the UBL domains of USP47 may also affect the substrate binding and have unique functions. However, further structural and functional studies are needed.

In the previous study, we determined the structures of the USP47 catalytic domain with and without ubiquitin bound to better understand its structural and functional characteristics and serve as a basis for the design of USP47-targeted compounds [36]. Based on the study, we conducted *in silico* virtual screening and selected K-552 (Figure S4 B-C). As expected, it is mainly targeting USP47 than USP7, unlike other USP47 inhibitor compounds discovered *in vitro* (Figure S4 D-G). Somewhat differently from *in vitro* findings, K-552 does not inactivate USP7 but instead inactivates USP47 in A549 cell lines (Fig. 4C, D). We hypothesize that K-552 was designed based on $USP47_{CD}$ structure, which may explain its high K_D value for $USP7_{CD}$ and consequent inability to effectively inactivate USP7. Furthermore, only the catalytic domain of recombinant USP47 and USP7 was used in the *in vitro* assay, suggesting that other domains may influence the activity of both USP47 and USP7 in a cellular context.

The recent FDA approval of Sotorasib marks a significant milestone in targeted therapy for KRAS-driven NSCLC and colorectal cancer [64], [65]. However, despite this advancement, ongoing research is focused on combination therapies to improve treatment outcomes and address acquired resistance [66]. Studies have mainly focused on a synergistic effect whereby downstream components of the KRAS pathway are inhibited to overcome resistance and enhance the effectiveness of KRAS G12C inhibitors. The stability of the c-Myc protein, which we identified as a substrate of USP47, is enhanced through the oncogenic RAS signaling pathway [3,4,15]. Recently, c-Myc, one of the RAS downstream molecules, was found to be a key molecule of $KRAS^{G12Ci}$ sensitivity and resistance *in vitro* and *in vivo* models [4,15]. In PDAC cells which shows insensitivity of Sotorasib, oncogenic KRAS promotes c-Myc protein stability by ERK/Survivin axis. Researchers targeted survivin to suppress c-Myc protein level by regulating phosphorylation, thereby inhibiting the proliferation of PDAC cell line with mutated KRAS [4]. According to Wang et al., PLK1 was elevated and promoted c-Myc phosphorylation to stabilize the c-Myc protein in $KRAS^{G12Ci}$ -resistant cell line [15]. Both studies focused on targeting proteins that regulate c-Myc protein stability. Furthermore, previous studies indicated that the abundance of c-Myc is associated with $KRAS^{G12Ci}$ insensitivity in clinical practice [7]. Analysis of patient samples from clinical practice revealed that three patients treated with Sotorasib exhibited genetic alterations in c-Myc, leading to Myc amplification [7]. Based on these findings, we hypothesized USP47-c-Myc axis could be a potential pathway to enhance the effectiveness of $KRAS^{G12Ci}$ Sotorasib.

Recent studies have also suggested that the modulation of protein homeostasis is a mechanism for tumors to gain resistance in response to oncogenic KRAS inhibitors. Inotisol-requiring enzyme 1α (IRE1α) has been identified as a key node in proteostasis reprogramming, and inhibiting IRE1α enhances the response of $KRAS^{G12C}$-driven tumors to Sotorasib [67]. Our study implies that other enzymes that regulate protein homeostasis could also be key in overcoming resistance or enhancing sensitivity to KRAS inhibitors. Altogether, we determined that modulating c-Myc protein degradation by inhibiting USP47 could be an effective way to enhance the response of $KRAS^{G12}$- mutated cancer cells to Sotorasib.

We investigated whether combining K-552 with Sotorasib could enhance the sensitivity of $KRAS^{G12Ci}$ in lung cancer. First, to study the additional effect of Sotorasib with a USP47 inhibitor *in vitro*, we selected three KRAS G12C-mutated cell lines based on previous studies [49,68], which indicated that Calu-1 and H1171 are less sensitive than H358. Cell viability in the Calu-1 or H1171 cell lines is still greater than fifty

percent even when cells are treated with Sotorasib at 1 or 10 μM [49,68]. We also found that K-552, USP47 inhibitor showed poor responses in Calu-1 and HCC1171 cell lines, with IC_{50} value 42.95 μM and 50.77 μM, respectively (Fig. 4I, J). Therefore, we hypothesized that Calu-1 and H358 would exhibit an enhanced combinatorial response to Sotorasib (at 0.1 or 1 μM) and K-552 (at 25 μM), at lower concentrations than those used in monotherapy. Indeed, Sotorasib treatment was more effective in USP47 knockdown cells compared to USP47-expressed cell lines (Fig. 5A-C). Likewise, the co-treatment of Sotorasib and K-552 had an additive effect in inhibiting $KRAS^{G12C}$ mutated NSCLC cell lines (Fig. 5D-F). As expected, the BSS scores for Calu-1 cells indicated combinational effects with at least 0.1 μM Sotorasib and 25 μM K-552, while HCC1171 cells showed synergistic effects with at least 1 μM Sotorasib and 25 μM K-552. For H358, a cell line sensitive to Sotorasib, a synergistic effect on cell viability was at 0.01 μM Sotorasib and 12.5 μM K-552.

To elucidate the mechanism of the combination therapy, we observed that concomitant treatment with Sotorasib and K-552 additionally attenuated c-Myc protein levels and induced apoptosis (Fig. 5G-H, J). We also acknowledged that EMT is a compelling cause of $KRAS^{G12Ci}$ resistance [8,49]. It was also reported that USP47 is one of the factors of EMT [24]. Consistent with a previous study on the relation between USP47 and EMT, the combination of Sotorasib and K-552 reduces EMT marker protein levels (Fig. 5K).

Most identified USP47 inhibitors primarily target USP7. P5091 was the first compound identified as a USP7/USP47 dual inhibitor, and several derivatives have been developed for further optimization [69]. Among them, P50429 and P22077, derivatives of P5091, inhibit both USP7 and USP47 at lower concentrations compared to P5091. Parthenolide, which is derived from the leaves of feverfew (*Tanacetum parthenium*), has been traditionally used for relieving fever, migraine, and inflammation. It has also demonstrated anti-cancer effects [33,70]. Parthenolide, identified as a USP7 inhibitor, has been shown to bind and inhibit USP47 as well [28]. Compared to other USP47 inhibitors, such as P50429, K-552 demonstrates specificity, which may minimize off-target effects. However, resistance to K-552 could arise through compensatory activation of alternative pathways or adaptive feedback loops within the KRAS signaling network. Notably, USP47 regulates multiple substrates linked to key oncogenic pathways, including NF-κB and PI3K/AKT, suggesting that its inhibition could modulate broader signaling networks. Other DUB inhibitors, such as b-AP15/VLX1570 and inhibitors of USP14 and UCHL5, have also been reported to develop moderate resistance *in vitro* [71]. Therefore, investigating combination strategies, such as co-targeting USP47 with MEK or PI3K inhibitors, and conducting direct comparative studies with other USP47 inhibitors are essential for optimizing therapeutic efficacy. Future studies should also explore structure-activity relationships to further enhance specificity and develop second-generation inhibitors with improved potency and safety profiles.

In summary, our study highlights that USP47 plays an essential role in enhancing oncoprotein c-Myc and promoting cell proliferation in lung cancers. Targeting USP47 with K-552 sensitizes KRAS G12C-mutated NSCLC cells to Sotorasib by reducing c-Myc protein levels. The collaborative use of Sotorasib and K-552 enhances cytotoxicity, induces apoptosis, and reduces mesenchymal transition by concomitantly targeting and inducing c-Myc proteasomal degradation pathways in KRAS-mutated cells (Fig. 7). Therefore, we suggest that targeting USP47 is a promising strategy for overcoming the limitations of $KRAS^{G12Ci}$, although more research is necessary to develop more optimized USP47 inhibitors for treating KRAS-mutated NSCLC.

CRediT authorship contribution statement

Song Eun Joo: Writing – review & editing, Writing – original draft,

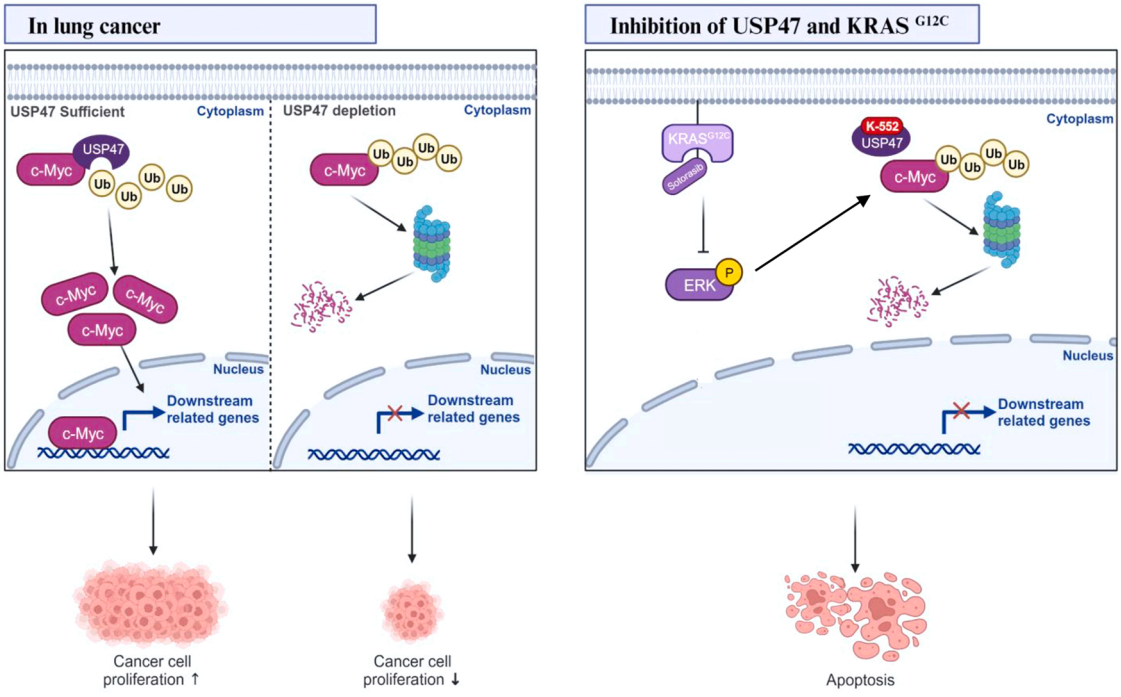


Fig. 7. Molecular mechanism of USP47 inhibition and $KRAS^{G12Ci,}$ The scheme illustrates the mechanism of USP47 and c-Myc interaction in non-small cell lung cancer (NSCLC) and the therapeutic effect of combining K-552 and Sotorasib. In NSCLC cells with high USP47 expression, USP47 interacts with and deubiquitinates c-Myc, stabilizing the c-Myc protein and promoting cancer cell proliferation. When USP47 is depleted or inhibited, c-Myc remains ubiquitinated, leading to its degradation via the proteasomal pathway, thus reducing cancer cell proliferation. In $KRAS^{G12C}$-mutated cancer cells, K-552 blocks USP47 activity, destabilizing c-Myc and inducing its proteasomal degradation. Concurrently, Sotorasib targets the $KRAS^{G12C}$ mutation, suppressing ERK phosphorylation and reducing c-Myc stability, both of which are critical downstream effects of KRAS signaling. The combination of K-552 (USP47 inhibitor) and Sotorasib ($KRAS^{G12C}$ inhibitor) demonstrates a synergistic effect by promoting apoptosis through inhibition of c-Myc stabilization. The figure was generated using BioRender.

Supervision, Funding acquisition, Conceptualization. **Jeong Jeong Hyun:** Methodology, Investigation. **Shin Sang Chul:** Methodology, Investigation. **Shin Hyungkyung:** Writing – original draft, Methodology, Investigation, Conceptualization. **Hwang SuA:** Visualization, Methodology, Investigation. **Hwang Inah:** Methodology. **Kim Eunice EunKyeong:** Writing – review & editing, Supervision, Resources, Methodology, Investigation. **Oh Yeonji:** Investigation. **Kim Jinhyeok:** Investigation. **Choo Hyunah:** Writing – review & editing, Resources, Methodology, Investigation, Funding acquisition.

Declaration of Competing Interest

The authors declare that they have no known competing financial interests or personal relationships that could have appeared to influence the work reported in this paper.

Acknowledgements

This work was supported by a National Research Foundation of Korea (NRF) grant funded by the Korean government (MSIP) (RS-2024–00338237) and by a Korea Basic Science Institute (National Research Facilities and Equipment Center) grant, funded by the Ministry of Education (2021R1A6C101A442). This work is additionally funded by Korea Institute of Science and Technology (KIST) Institutional Program (2E33791 and 2V10210) and was supported by a grand of Korean ARPA-H Project through the Korea Health Industry Development Institute (KHIDI), funded by the Ministry of Health & Welfare, Republic of Korea (RS-2024–00512595)

Appendix A. Supporting information

Supplementary data associated with this article can be found in the online version at doi:10.1016/j.phrs.2025.107722.

Data Availability

Data will be made available on request.

References

[1] R.L. Siegel, K.D. Miller, N.S. Wagle, A. Jemal, Cancer statistics, 2023, CA Cancer J. Clin. 73 (1) (2023) 17–48.
[2] R.S. Herbst, D. Morgensztern, C. Boshoff, The biology and management of non-small cell lung cancer, Nature 553 (7689) (2018) 446–454.
[3] A.V. Vaseva, D.R. Blake, T.S.K. Gilbert, S. Ng, G. Hostetter, S.H. Azam, et al., KRAS suppression-induced degradation of MYC is antagonized by a MEK5-ERK5 compensatory mechanism, Cancer Cell 34 (5) (2018) 807.
[4] W.H. Chang, Y. Liu, E.A. Hammes, K.L. Bryant, R.A. Cerione, M.A. Antonyak, Oncogenic RAS promotes MYC protein stability by upregulating the expression of the inhibitor of apoptosis protein family member Survivin, J. Biol. Chem. 299 (2) (2023) 102842.
[5] J. Canon, K. Rex, A.Y. Saiki, C. Mohr, K. Cooke, D. Bagal, et al., The clinical KRAS (G12C) inhibitor AMG 510 drives anti-tumour immunity, Nature 575 (7781) (2019) 217–223.
[6] F. Skoulidis, B.T. Li, G.K. Dy, T.J. Price, G.S. Falchook, J. Wolf, et al., Sotorasib for lung cancers with KRAS p.G12C mutation, N. Engl. J. Med. 384 (25) (2021) 2371–2381.
[7] Y. Zhao, Y.R. Murciano-Goroff, J.Y. Xue, A. Ang, J. Lucas, T.T. Mai, et al., Diverse alterations associated with resistance to KRAS(G12C) inhibition, Nature 599 (7886) (2021) 679–683.
[8] W. Ning, T.M. Marti, P. Dorn, R.W. Peng, Non-genetic adaptive resistance to KRAS (G12C) inhibition: EMT is not the only culprit, Front Oncol. 12 (2022) 1004669.
[9] A. Federico, I. Ricciotti, V. Favorito, S.V. Michelina, P. Scaparone, G. Metro, et al., Resistance to KRAS G12C inhibition in non-small cell lung cancer, Curr. Oncol. Rep. 25 (9) (2023) 1017–1029.
[10] S.L. Tammaccaro, P. Prigent, J.C. Le Bail, O. Dos-Santos, L. Dassencourt, M. Eskandar, et al., TEAD inhibitors sensitize KRAS inhibitors via dual cell cycle arrest in KRAS-mutant NSCLC, Pharmaceuticals 16 (4) (2023) 553.
[11] P. Barrios-Bernal, J. Lucio-Lozada, M. Ramos-Ramírez, N. Hernández-Pedro, O. Arrieta, A novel combination of sotorasib and metformin enhances cytotoxicity and apoptosis in KRAS-mutated non-small cell lung cancer cell lines through MAPK and P70S6K inhibition, Int. J. Mol. Sci. 24 (5) (2023) 4331.
[12] S. Khan, J. Wiegand, P. Zhang, W. Hu, D. Thummuri, V. Budamagunta, et al., BCL-X(L) PROTAC degrader DT2216 synergizes with sotorasib in preclinical models of KRAS(G12C)-mutated cancers, J. Hematol. Oncol. 15 (1) (2022) 23.
[13] N. Hondo, M. Kitazawa, M. Koyama, S. Nakamura, S. Tokumaru, S. Miyazaki, et al., MEK inhibitor and anti-EGFR antibody overcome sotorasib resistance signals and enhance its antitumor effect in colorectal cancer cells, Cancer Lett. 567 (2023) 216264.
[14] M. Maqbool, M.S. Hussain, A.S. Bisht, A. Kumari, A. Kamran, A. Sultana, et al., Connecting the dots: LncRNAs in the KRAS pathway and cancer, Pathol. Res. Pract. 262 (2024) 155570.
[15] Y. Wang, M. Yao, C. Li, K. Yang, X. Qin, L. Xu, et al., Targeting ST8SIA6-AS1 counteracts KRAS(G12C) inhibitor resistance through abolishing the reciprocal activation of PLK1/c-Myc signaling, Exp. Hematol. Oncol. 12 (1) (2023) 105.
[16] E.V. Schmidt, The role of c-myc in cellular growth control, Oncogene 18 (19) (1999) 2988–2996.
[17] P. Sunpaweravong, P. Thongwatchara, R. Chotipanvithayakul, S. Sangkhathat, P. Thongsuksai, Expression and prognostic significance of c-Myc, ALK, ROS1, BRAF, and PD-L1 among patients with non-small cell lung cancer, Clin. Med Insights Oncol. 16 (2022) pp.11795549221092747.
[18] P. Sunpaweravong, P. Thongwatchara, R. Chotipanvithayakul, S. Sangkhathat, P. Thongsuksai, Copy number gains of chromosome 17 identified by dual in situ hybridization in non-small cell lung cancer tissue correlate with overexpression of c-Myc, Transl. Cancer Res 11 (5) (2022) 1033–1044.
[19] M. Yada, S. Hatakeyama, T. Kamura, M. Nishiyama, R. Tsunematsu, H. Imaki, et al., Phosphorylation-dependent degradation of c-Myc is mediated by the F-box protein Fbw7, EMBO J. 23 (10) (2004) 2116–2125.
[20] H. Chen, H. Liu, G. Qing, Targeting oncogenic Myc as a strategy for cancer treatment, Signal Transduct. Target Ther. 3 (1) (2018) 5.
[21] T. Das, S.C. Shin, E.J. Song, E.E. Kim, Regulation of deubiquitinating enzymes by post-translational modifications, Int J. Mol. Sci. 21 (11) (2020).
[22] Y.J. Kim, Y. Lee, H. Shin, S. Hwang, J. Park, E.J. Song, Ubiquitin-proteasome system as a target for anticancer treatment-an update, Arch. Pharm. Res. 46 (7) (2023) 573–597.
[23] K. Pan, J. Fu, W. Xu, Role of ubiquitin-specific peptidase 47 in cancers and other diseases, Front. Cell Dev. Biol. 9 (2021) 726632.
[24] V.C. Silvestrini, C.H. Thome, D. Albuquerque, C. de Souza Palma, G.A. Ferreira, G. P. Lanfredi, et al., Proteomics analysis reveals the role of ubiquitin specific protease (USP47) in Epithelial to Mesenchymal Transition (EMT) induced by TGFbeta2 in breast cells, J. Proteom. 219 (2020) 103734.
[25] H. Lei, H.Z. Xu, H.Z. Shan, M. Liu, Y. Lu, Z.X. Fang, et al., Targeting USP47 overcomes tyrosine kinase inhibitor resistance and eradicates leukemia stem/progenitor cells in chronic myelogenous leukemia, Nat. Commun. 12 (1) (2021) 51.
[26] J. Yang, E.L. Weisberg, S. Qi, W. Ni, H. Mei, Z. Wang, et al., Inhibition of the deubiquitinating enzyme USP47 as a novel targeted therapy for hematologic malignancies expressing mutant EZH2, Leukemia 36 (4) (2022) 1048–1057.
[27] J. Peng, W. Li, N. Tan, X. Lai, W. Jiang, G. Chen, USP47 stabilizes BACH1 to promote the Warburg effect and non-small cell lung cancer development via stimulating Hk2 and Gapdh transcription, Am. J. Cancer Res. 12 (1) (2022) 91–107.
[28] S. Zhang, X. Ju, Q. Yang, Y. Zhu, D. Fan, G. Su, et al., USP47 maintains the stemness of colorectal cancer cells and is inhibited by parthenolide, Biochem. Biophys. Res. Commun. 562 (2021) 21–28.
[29] B. Pan, Y. Yang, J. Li, Y. Wang, C. Fang, F.X. Yu, Y. Xu, USP47-mediated deubiquitination and stabilization of YAP contributes to the progression of colorectal cancer, Protein Cell 11 (2) (2020) 138–143.
[30] J. Cho, J. Park, S.C. Shin, M. Jang, J.H. Kim, E.E. Kim, E.J. Song, USP47 promotes tumorigenesis by negative regulation of p53 through deubiquitinating ribosomal protein S2, Cancers 12 (5) (2020).
[31] J. Park, M. Cho, J. Cho, E.E. Kim, E.J. Song, MicroRNA-101-3p suppresses cancer cell growth by inhibiting the USP47-induced deubiquitination of RPL11, Cancers 14 (4) (2022) 964.
[32] D. Ashton-Beaucage, C. Lemieux, C.M. Udell, M. Sahmi, S. Rochette, M. Therrien, The deubiquitinase USP47 stabilizes MAPK by counteracting the function of the N-end rule ligase POE/UBR4 in drosophila, PLoS Biol. 14 (8) (2016) e1002539.
[33] X. Li, L. Kong, Q. Yang, A. Duan, X. Ju, B. Cai, et al., Parthenolide inhibits ubiquitin-specific peptidase 7 (USP7), Wnt signaling, and colorectal cancer cell growth, J. Biol. Chem. 295 (11) (2020) 3576–3589.
[34] J. Park, J. Cho, E.J. Song, Ubiquitin-proteasome system (UPS) as a target for anticancer treatment, Arch. Pharm. Res. 43 (11) (2020) 1144–1161.
[35] P.S. Ramalingam, T. Premkumar, V. Sundararajan, M.S. Hussain, S. Arumugam, Design and development of dual targeting CAR protein for the development of CAR T-cell therapy against KRAS mutated pancreatic ductal adenocarcinoma using computational approaches, Discov. Oncol. 15 (1) (2024) 592.
[36] S.C. Shin, J. Park, K.H. Kim, J.M. Yoon, J. Cho, B.H. Ha, et al., Structural and functional characterization of USP47 reveals a hot spot for inhibitor design, Commun. Biol. 6 (1) (2023) 970.
[37] S.Y. Park, H. Choi, S.M. Choi, S. Wang, S. Shim, W. Jun, et al., T-plastin contributes to epithelial-mesenchymal transition in human lung cancer cells through FAK/AKT/Slug axis signaling pathway, BMB Rep. 57 (6) (2024) 305–310.
[38] M. Nagasaka, Y. Inoue, M. Yoshida, C. Miyajima, D. Morishita, M. Tokugawa, et al., The deubiquitinating enzyme USP17 regulates c-Myc levels and controls cell proliferation and glycolysis, FEBS Lett. 596 (4) (2022) 465–478.
[39] E.M. Glare, M. Divjak, M.J. Bailey, E.H. Walters, beta-Actin and GAPDH housekeeping gene expression in asthmatic airways is variable and not suitable for normalising mRNA levels, Thorax 57 (9) (2002) 765–770.

[40] A.P. Turnbull, S. Ioannidis, W.W. Krajewski, A. Pinto-Fernandez, C. Heride, A.C. L. Martin, et al., Molecular basis of USP7 inhibition by selective small-molecule inhibitors, Nature 550 (7677) (2017) 481–486.
[41] W.N. Arifin, W.M. Zahiruddin, Sample size calculation in animal studies using resource equation approach, Malays. J. Med. Sci. 24 (5) (2017) 101–105.
[42] F. Faul, E. Erdfelder, A.-G. Lang, A. Buchner, G*Power 3: a flexible statistical power analysis program for the social, behavioral, and biomedical sciences, Behav. Res. Methods 39 (2) (2007) 175–191.
[43] Y. Li, P. Xie, L. Lu, J. Wang, L. Diao, Z. Liu, et al., An integrated bioinformatics platform for investigating the human E3 ubiquitin ligase-substrate interaction network, Nat. Commun. 8 (1) (2017) 347.
[44] G. Benstead-Hume, X. Chen, S.R. Hopkins, K.A. Lane, J.A. Downs, F.M.G. Pearl, Predicting synthetic lethal interactions using conserved patterns in protein interaction networks, PLoS Comput. Biol. 15 (4) (2019) e1006888.
[45] M. Altun, H.B. Kramer, L.I. Willems, J.L. McDermott, C.A. Leach, S.J. Goldenberg, et al., Activity-based chemical proteomics accelerates inhibitor development for deubiquitylating enzymes, Chem. Biol. 18 (11) (2011) 1401–1412.
[46] A. Pozhidaeva, G. Valles, F. Wang, J. Wu, D.E. Sterner, P. Nguyen, et al., USP7-specific inhibitors target and modify the enzyme's active site via distinct chemical mechanisms, Cell Chem. Biol. 24 (12) (2017) 1501–1512, e1505.
[47] E. O'Sullivan, A. Keogh, B. Henderson, S.P. Finn, S.G. Gray, K. Gately, Treatment strategies for KRAS-mutated non-small-cell lung cancer, Cancers 15 (6) (2023).
[48] L. Yu, J. Fu, C. Shen, Ubiquitin specific peptidase 47 promotes proliferation of lung squamous cell carcinoma, Genes Genom. 44 (6) (2022) 721–731.
[49] Y. Adachi, K. Ito, Y. Hayashi, R. Kimura, T.Z. Tan, R. Yamaguchi, H. Ebi, Epithelial-to-mesenchymal transition is a cause of both intrinsic and acquired resistance to KRAS G12C inhibitor in KRAS G12C-mutant non-small cell lung cancer, Clin. Cancer Res 26 (22) (2020) 5962–5973.
[50] A. Mohanty, A. Nam, S. Srivastava, J. Jones, B. Lomenick, S.S. Singhal, et al., Acquired resistance to KRAS G12C small-molecule inhibitors via genetic/nongenetic mechanisms in lung cancer, Sci. Adv. 9 (41) (2023) eade3816.
[51] S. Zheng, W. Wang, J. Aldahdooh, A. Malyutina, T. Shadbahr, Z. Tanoli, et al., SynergyFinder plus: toward better interpretation and annotation of drug combination screening datasets, Genom. Proteom. Bioinforma. 20 (3) (2022) 587–596.
[52] Y. Hu, Z. Ma, Z. Chen, B. Chen, USP47 promotes apoptosis in rat myocardial cells after ischemia/reperfusion injury via NF-κB activation, Biotechnol. Appl. Biochem 68 (4) (2021) 841–848.
[53] Q. Guo, Y. Jin, X. Chen, X. Ye, X. Shen, M. Lin, et al., NF-κB in biology and targeted therapy: new insights and translational implications, Signal Transduct. Target. Ther. 9 (1) (2024) 53.
[54] N. Popov, M. Wanzel, M. Madiredjo, D. Zhang, R. Beijersbergen, R. Bernards, et al., The ubiquitin-specific protease USP28 is required for MYC stability, Nat. Cell Biol. 9 (7) (2007) 765–U771.
[55] S. Bhattacharya, M.K. Ghosh, HAUSP regulates c-MYC expression via de-ubiquitination of TRRAP, Cell Oncol. (Dordr.) 38 (4) (2015) 265–277.
[56] J. Pan, Q. Deng, C. Jiang, X. Wang, T. Niu, H. Li, et al., USP37 directly deubiquitinates and stabilizes c-Myc in lung cancer, Oncogene 34 (30) (2015) 3957–3967.
[57] X.X. Sun, X. He, L. Yin, M. Komada, R.C. Sears, M.S. Dai, The nucleolar ubiquitin-specific protease USP36 deubiquitinates and stabilizes c-Myc, Proc. Natl. Acad. Sci. USA 112 (12) (2015) 3734–3739.
[58] M. Li, J. Yu, L. Ju, Y. Wang, W. Jin, R. Zhang, et al., USP43 stabilizes c-Myc to promote glycolysis and metastasis in bladder cancer, Cell Death Dis. 15 (1) (2024) 44.
[59] Y. Peng, J. Liu, Z. Wang, C. Cui, T. Zhang, S. Zhang, et al., Prostate-specific oncogene OTUD6A promotes prostatic tumorigenesis via deubiquitinating and stabilizing c-Myc, Cell Death Differ. (2022).
[60] M. Welcker, B. Wang, D.V. Rusnac, Y. Hussaini, J. Swanger, N. Zheng, B. E. Clurman, Two diphosphorylated degrons control c-Myc degradation by the Fbw7 tumor suppressor, Sci. Adv. 8 (4) (2022) eabl7872.
[61] T.S. Bekaii-Saab, R. Yaeger, A.I. Spira, M.S. Pelster, J.K. Sabari, N. Hafez, et al., Adagrasib in Advanced Solid Tumors Harboring a KRAS(G12C) Mutation, J. Clin. Oncol. 0 (ja) (2023) pp.101200JCO2300434.
[62] A.C. Faesen, A.M. Dirac, A. Shanmugham, H. Ovaa, A. Perrakis, T.K. Sixma, Mechanism of USP7/HAUSP activation by its C-terminal ubiquitin-like domain and allosteric regulation by GMP-synthetase, Mol. Cell 44 (1) (2011) 147–159.
[63] M. Clerici, M.P. Luna-Vargas, A.C. Faesen, T.K. Sixma, The DUSP-Ubl domain of USP4 enhances its catalytic efficiency by promoting ubiquitin exchange, Nat. Commun. 5 (1) (2014) 5399.
[64] D.S. Hong, M.G. Fakih, J.H. Strickler, J. Desai, G.A. Durm, G.I. Shapiro, et al., KRASG12C inhibition with sotorasib in advanced solid tumors, N. Engl. J. Med. 383 (13) (2020) 1207–1217.
[65] F. Skoulidis, B.T. Li, G.K. Dy, T.J. Price, G.S. Falchook, J. Wolf, et al., Sotorasib for lung cancers with KRAS p. G12C mutation, N. Engl. J. Med. 384 (25) (2021) 2371–2381.
[66] Y. Adachi, K. Ito, Y. Hayashi, R. Kimura, T.Z. Tan, R. Yamaguchi, H. Ebi, Epithelial-to-mesenchymal transition is a cause of both intrinsic and acquired resistance to KRAS G12C inhibitor in KRAS G12C–mutant non–small cell lung cancer, Clin. Cancer Res. 26 (22) (2020) 5962–5973.
[67] X. Lv, X. Lu, J. Cao, Q. Luo, Y. Ding, F. Peng, et al., Modulation of the proteostasis network promotes tumor resistance to oncogenic KRAS inhibitors, Science 381 (6662) (2023) eabn4180.
[68] H. Kitai, P.H. Choi, Y.C. Yang, J.A. Boyer, A. Whaley, P. Pancholi, et al., Combined inhibition of KRASG12C and mTORC1 kinase is synergistic in non-small cell lung cancer, Nat. Commun. 15 (1) (2024) 6076.
[69] J. Weinstock, J. Wu, P. Cao, W.D. Kingsbury, J.L. McDermott, M.P. Kodrasov, et al., Selective dual inhibitors of the cancer-related deubiquitylating proteases USP7 and USP47, ACS Med. Chem. Lett. 3 (10) (2012) 789–792.
[70] S. Zhu, P. Sun, S. Bennett, O. Charlesworth, R. Tan, X. Peng, et al., The therapeutic effect and mechanism of parthenolide in skeletal disease, cancers, and cytokine storm, Front Pharm. 14 (2023) 1111218.
[71] P.-M. Chow, J.-R. Dong, Y.-W. Chang, K.-L. Kuo, W.-C. Lin, S.-H. Liu, K.-H. Huang, The UCHL5 inhibitor b-AP15 overcomes cisplatin resistance via suppression of cancer stemness in urothelial carcinoma, Mol. Ther. Oncolyt. 26 (2022) 387–398.